Hippocampus-lateral septum circuitry mediates memory for food location in rats

Elizabeth A. Davis[1*], Clarissa M. Liu[1,2*], Isabella H. Gianatiempo[1], Andrea N. Suarez[1], Alyssa M. Cortella[1], Joel D. Hahn[3], and Scott E. Kanoski[1,2]

[*]These two authors contributed equally

[1]Human and Evolutionary Biology Section, Department of Biological Sciences, Dornsife College of Letters, Arts and Sciences, University of Southern California, 3616 Trousdale Pkwy, Los Angeles, CA, USA, 90089; [2]Neuroscience Graduate Program, University of Southern California, 3641 Watt Way, Los Angeles, CA, USA. 90089; [3]Neurobiology Section, Department of Biological Sciences, Dornsife College of Letters, Arts and Sciences, University of Southern California, 3616 Trousdale Pkwy, Los Angeles, CA, USA, 90089

Corresponding author:
Scott E. Kanoski, PhD
University of Southern California
3616 Trousdale Parkway, AHF-252
Los Angeles, CA 90089-0372
Phone: 213-821-5762
Email: kanoski@usc.edu

Classification: Biological Sciences, Neuroscience

Keywords: feeding, cognition, place cells, motivation, reward, foraging, lateral hypothalamic area, prefrontal cortex

ABSTRACT

Remembering the location of a food source is essential for securing energy for survival. Here we identify a hippocampal-septal neural circuit that controls food-directed spatial memory. Both reversible and chronic disconnection of ventral hippocampus CA1 subregion (CA1v) projections to the lateral-septum (LS) using pathway-specific dual viral approaches impaired memory retention in a spatial food-seeking foraging task in rats. However, disconnection of this pathway did not affect performance in an aversive escape-motivated spatial memory task that used the same apparatus and visuospatial cues, suggesting that CA1v-LS signaling selectively mediates spatial memory for food location vs. spatial memory in general. The selectivity of this pathway in mediating foraging-related spatial memory was further supported by results showing that CA1v-LS disconnection did not affect anxiety-like behavior, locomotor activity, or social and olfactory-based appetitive learning. To examine whether CA1v-LS mediation of foraging-related spatial memory involves collateral projections of CA1v neurons, we utilized virus-based neural pathway tracing analyses to identify the mPFC as a collateral target of LS-projecting CA1v neurons. However, functional disconnection of the CA1v and mPFC did not affect spatial memory for food location, thus further supporting the selectivity of CA1v-LS signaling for this behavior. The nucleus accumbens, lateral hypothalamic area, and other brain regions associated with food motivation and reward were identified as second-order targets of CA1v-LS signaling using a multisynaptic anterograde tracing approach. Collective results reveal that CA1v to LS communication plays a critical role in remembering the environmental location of food, thus identifying a novel neural pathway regulating foraging-related memory processes.

INTRODUCTION

A survival advantage common to early humans and lower-order mammals is to accurately remember the location of a food source in the environment, and to then efficiently navigate back to a shelter or other safe location. The neurobiological substrates that regulate visuospatial navigation are therefore critical to effectively implement food-directed foraging behavior. Brain structures within the telencephalon have been identified as being essential for visuospatial mapping and egocentric orientation in the environment, including the hippocampus and the medial entorhinal cortex, respectively (1, 2). However, despite that reliably locating food in the environment is a key selection pressure driving the evolution of visuospatial navigation, the overwhelming majority of rodent model research on the substrates of spatial learning and memory have utilized procedures such as the Morris water maze and the Barnes maze that each involve escaping aversive reinforcement (3, 4). Furthermore, while single unit recordings have been used to identify specific populations of neurons that subserve distinct navigational functions (e.g., hippocampal "place cells", medial entorhinal "grid cells")(5, 6), the bulk of this research has recorded neural activity under neutral conditions void of either appetitive or aversive reinforcement. Very little research has been dedicated to identify brain regions and neural circuits that may specifically promote food-directed spatial memory, as well as the extent to which the nature of the reinforcement is a critical factor in deciphering the brain's control of visuospatial navigation.

The majority of rodent model research investigating brain regions that mediate visuospatial navigational memory has focused on the anterior and "dorsal" subregion of the hippocampus (septal pole; HPCd). However, the posterior and "ventral" hippocampus subregion (temporal pole; HPCv), while classically associated with stress- and affect-associated memory processes (7), also plays a role in visuospatial learning and memory (8-10). For example, under some testing conditions selective HPCv lesions impair spatial memory performance in the Morris water maze (10, 11). Moreover, place cells that are responsive to changes in the visuospatial environment are present within both the HPCd and HPCv pyramidal layers, with a linear increase in the scale of representation from the dorsal to the ventral pole (9). Despite a common role for the HPCd and HPCv in mediating spatial memory, there is also evidence for a functional distinction between the subregions (7, 12, 13). For instance, lesions of the HPCv but not the

HPCd alter stress responses (14) and anxiety-like behavior (15), whereas HPCd but not HPCv lesions impair spatial memory in an incidental (nonreinforced) procedure (16). These two HPC subregions also have distinct afferent and efferent neural connections. This disparate neuroanatomical connectivity supports a framework for a functional diversity in which the HPCd preferentially processes cortical-derived sensory information and the HPCv preferentially processes metabolic and limbic-derived affective information (7, 13). The functional distinction between these two subregions is further supported by the generation of the hippocampus gene expression atlas, which provides a comprehensive integration of gene expression and connectivity across the HPC axis (17). Given that both the HPCv and the HPCd participate in spatial memory but have distinct neuroanatomical connectivity and contributions when it comes to regulating other cognitive and mnemonic processes, it is feasible that the HPCv and HPCd support different forms of spatial memory depending on the type of reinforcement or context associated with the behavior.

Recent findings identify the HPCv as a critical brain substrate in regulating feeding behavior and food-directed memory processes. Reversible inactivation of HPCv neurons after a meal increases the size of and reduces the latency to consume a subsequent meal (18, 19). In addition, receptors for feeding-related hormones are more abundantly expressed in the HPCv compared to the HPCd (e.g., ghrelin receptors (20, 21), glucagon-like peptide-1 [GLP-1] receptors (22)), and these HPCv endocrine receptor systems alter food intake and feeding-related memory (23). For example, leptin and GLP-1 act in the HPCv (CA1v subregion) to decrease food intake and food-motivated conditioned behaviors (24-26), whereas the orexigenic gut-derived hormone ghrelin administered to the HPCv but not HPCd has opposite effects (23, 27). Olfactory information, which is intimately connected with feeding behavior, is also preferentially processed within the HPCv compared with the HPCd. The CA1v, specifically, is bidirectionally connected to brain regions that process olfactory information (7, 28, 29), and CA1v neurons respond more robustly to olfactory contextual cues compared with CA1d (8). Further, ghrelin signaling in the CA1v improves olfactory- and socially-mediated memory for food preference (30). Given the HPCv appetite-relevant neuroanatomical connections, endocrine and neuropeptide receptor expression profiles, and functional evidence linking this subregion with food-motivated behaviors, we hypothesize that HPCv mediation of visuospatial memory is preferentially biased to food-reinforced foraging behavior.

94 HPCv pyramidal neurons have extensive projection targets throughout the brain (31), yet
95 the functional relevance of these pathways is poorly understood. Recently, a vHPC dentate
96 gyrus-CA3v to lateral septum (LS) pathway was identified that suppresses feeding (32).
97 Similarly, CA1v projections to the medial prefrontal cortex (mPFC) and lateral hypothalamic
98 area (LHA) mediate feeding-related outcomes associated with GLP-1 and ghrelin signaling,
99 respectively. CA1v neurons also robustly target the LS (33, 34), however, the relevance of this
100 pathway to feeding behavior and/or feeding-related memory is unknown. It is feasible that CA1v
101 to LS projections participate in regulating spatial memory for food location, a notion supported
102 by findings showing that neuroplastic changes occur in the LS after learning a spatial memory
103 task (35, 36). Thus, in addition to exploring the role of the HPCv in memory for the spatial
104 location of food, the present study also investigated the specific role of the CA1v to LS pathway
105 in foraging-relevant memory processes.
106 To systematically investigate the role of the HPCv and CA1v to LS signaling in
107 visuospatial learning and memory for food reinforcement, we developed a novel appetitive
108 reinforcement-based spatial foraging behavioral task that allows for direct comparison with an
109 aversive reinforcement-based task of similar difficulty that uses the same apparatus and spatial
110 cues. Performance in these tasks was assessed following pathway-specific dual viral-based
111 reversible (chemogenetic inhibition) or chronic (targeted apoptosis) disconnection of the CA1v
112 to LS pathway. To further expand neural network knowledge on CA1v to LS signaling, we used
113 conditional viral-based neuroanatomical tracing strategies to identify both first-order collateral
114 and second-order targets of LS-projecting CA1v neurons. Collective results from the present
115 study identify novel neural circuitry of specific relevance to foraging behavior.
116
117 **RESULTS**
118
119 **The ventral hippocampus (HPCv) is required for remembering the spatial location of food**
120 To examine the importance of the HPCv in memory for the spatial location of food,
121 animals received bilateral *N*-Methyl-D-aspartate excitotoxic lesions of the HPCv (HPCv lesion
122 n=12) or bilateral sham injections (control n=12) (histological analyses for the neuron-specific
123 NeuN antigen in Fig. 1A) and were tested rats in a novel appetitive visuospatial memory task
124 developed in our lab. Results revealed no significant differences in errors (incorrect hole

125 investigations) (Fig. 1E) or latency to locate the food source hole (Fig. 1F) during training.
126 However, memory probe results show that animals with HPCv lesions decreased the ratio of
127 correct + adjacent / total holes explored in the first minute compared with controls (Figure 1G;
128 $p<0.05$, entire two minutes in Figure 1H). Post-surgical analyses of food intake (Supp. Fig. 1A)
129 and body weight (Supp. Fig. 1B) found no group differences in these measures over time. These
130 collective results indicate the HPCv is required for memory retention but not learning of the
131 spatial location of food in the environment.
132
133 **Ventral hippocampus CA1 (CA1v) projections to the lateral septum (LS) mediate**
134 **appetitive spatial memory for food location, but not aversive spatial memory for escape**
135 **location**
136 A major neuroanatomical target of HPCv CA1 neurons (CA1v) is the LS (34). We
137 investigated the functional relevance of the CA1v to LS signaling in learning and recalling the
138 spatial location of food reinforcement using conditional dual viral approaches to either reversibly
139 (via cre-dependent pathway-specific inhibitory chemogenetics; diagram of approach in Fig. 2A)
140 or permanently (via cre-dependent pathway-specific caspase-induced lesions; diagram of
141 approach in Fig. 2B) disconnect CA1v to LS communication. Results from the appetitive spatial
142 memory task reveal no significant group differences during training in either errors before
143 locating the correct hole (Fig. 2E) or latency to locate the food source hole (Fig. 2F). However,
144 memory probe results demonstrate that both acute (pathway-specific DREADDs) and chronic
145 (pathway-specific caspase) CA1v to LS disconnection decreased the ratio of correct + adjacent /
146 total holes explored in the entire two minutes of the probe compared with controls (Fig. 2G;
147 $p<0.05$), with a similar trend in the first minute of the probe (Fig. 2H; $p=0.059$). Histological
148 analyses confirmed successful viral transfection of LS-projecting CA1v neurons with DREADDs
149 (Figs. 2C&D) or caspase (Supp. Figs. 2E&F), and post-surgical analyses of food intake (Supp.
150 Fig 2A) and body weight (Supp. Fig 2B) found no group differences in these measures over time.
151 These data demonstrate that CA1v to LS communication is critical for remembering the spatial
152 location of food, and that these effects are unlikely to be based on differences in energy status or
153 food motivation.
154 To evaluate whether the CA1v to LS pathway is specifically involved in food-related
155 spatial memory vs. spatial memory in general, in a separate cohort of animals we tested the effect

156 of reversible and chronic CA1v to LS disconnection in a spatial learning task based on aversive
157 reinforcement rather than food. Importantly, this task uses the same apparatus and visuospatial
158 cues as the spatial location food memory task described above, but the animals are motivated to
159 locate the tunnel to escape mildly aversive stimuli (bright lights, loud noise) with no food
160 reinforcement in the tunnel (see Fig. 1B). Training results revealed no significant group
161 differences in errors before correct hole (Fig. 2I) nor latency to locate the escape hole (Fig. 2J).
162 During the memory probe test, there were no group differences in the ratio of correct + adjacent /
163 total holes investigated during the first minute (Fig. 2K) nor the entire two minutes (Fig. 2L) of
164 the memory probe. Histological analyses confirmed successful viral transfection of LS-
165 projecting CA1v neurons with DREADDs (Figs. 2C&D) or caspase (Supp. Figs. 2E&F), and
166 post-surgical analyses of food intake (Supp. Fig. 2C) and body weight (Supp. Fig. 2D) found no
167 group differences in these measures over time. These collective findings suggest that CA1v to
168 LS signaling specifically mediates spatial memory in a reinforcement-dependent manner.
169

170 **CA1v to LS signaling does not participate in HPC-dependent nonspatial appetitive**
171 **memory, anxiety-like behavior, or levels of locomotor activity**

172 To examine the role of CA1v to LS signaling in a nonspatial food-reinforced memory
173 task, we tested the effect of reversible and chronic CA1v to LS disconnection in the social
174 transmission of food preference (STFP) test (diagram in Fig. 3A). The HPCv plays an important
175 role in STFP (30, 37, 38), which tests socially-mediated food-related memory based on previous
176 exposure to socially-communicated olfactory cues. Results revealed no differences in preference
177 ratio between groups (Fig. 3B), suggesting that neither acute nor chronic CA1v to LS
178 disconnection impair food-related memory based on social-based olfactory stimuli.

179 Hippocampal-septal circuitry has been shown to play a role in mediating anxiety and
180 stress behavior (39-41). Thus, we sought to confirm whether the observed foraging-related
181 memory impairments following CA1v-LS disconnection may be based, in part, on non-specific
182 behavioral effects of the disconnection procedures unrelated to memory, including anxiety-like
183 behavior (zero maze task; diagram of apparatus in Fig. 3C) and general locomotor activity (open
184 field test). Results showed no significant group differences in time spent in the open zones in the
185 zero maze test (Fig. 3D) nor in the number of open zone entries (Fig. 3E), suggesting that neither
186 chronic nor reversible disconnection of the CA1v to LS circuitry influences anxiety-like

behavior. In addition, CA1v to LS disconnection had no effect on general locomotor activity in the open field test (Fig. 3F). Overall these results indicate that that disconnection of CA1v to LS signaling does not affect nonspatial HPC-dependent appetitive memory in STFP, general locomotor activity, anxiety-like behavior, or locomotor activity.

The medial prefrontal cortex is a collateral target of LS-projecting CA1v neurons

In addition to the LS, CA1v neurons also robustly project to the medial prefrontal cortex (mPFC) and the lateral hypothalamic area, two pathways that we have previously shown to be involved in feeding behavior (25, 27, 42). To examine whether LS-projecting CA1v neurons have collateral targets in the mPFC, LHA, or in other brain regions, we utilized a conditional dual viral neural pathway tracing approach that identifies collateral targets of a specific monosynaptic pathway (CA1v->LS; diagram of approach in Fig. 4A, representative CA1v injection site in Fig. 4B, representative CA1v injection site in Fig. 4C). Results revealed that LS-projecting CA1v neurons also project to the mPFC (Fig. 4D), whereas minimal collateral labeling was observed in the LHA or in other brain regions (data not shown). Thus, it may be the case that the impaired spatial memory for food location observed following either reversible or chronic CA1v to LS disconnection are based, in part, on CA1v to mPFC signaling from the same CA1v to LS projecting neurons.

Neither CA1v to mPFC nor CA1v to LHA signaling contribute to spatial memory for food location

To test the functional relevance of the CA1v neural pathways that either do (CA1v to mPFC) or do not (CA1v to LHA) collateralize from CA1 to LS projections in food-directed spatial learning and memory, we took advantage of the exclusively ipsilateral projections from CA1v to mPFC (25) (and to LHA (42)) and used a 'contralesional' approach to functionally disconnect the CA1v to mPFC (or LHA) pathway (diagram of approach in Fig. 4E), while leaving CA1v and mPFC (or LHA) communication to other brain regions intact. Post-surgical analyses of food intake (Supp. Fig. 3A,C) and body weight (Supp. Fig. 3B,D) found no group differences in these measures over time. Training results from the appetitive spatial memory task revealed no group differences in errors before locating the correct hole (Fig. 4F, 4L) or latency to locate the food-baited hole (Fig. 4G, 4L) for either the CA1v-mPFC or the CA1v-LHA

218 disconnection groups. Memory probe results demonstrate that neither CA1v to mPFC nor CA1v
219 to LHA disconnection altered the ratio of correct + adjacent / total holes explored in the first
220 minute (Fig. 4H, 4M) or the entire two minutes (Fig. 4I, 4N) compared with controls. These data
221 collectively demonstrate that CA1v to LS mediation of foraging-related memory does not require
222 collateral projections to the mPFC neural pathway. Further, CA1v to LHA neural signaling,
223 although important for other food-related conditioned appetitive behaviors (27, 42), is not
224 required for either learning or remembering of the spatial location of food.
225
226 **Second-order targets of CA1v to LS neurons include the mPFC, the LHA, and the ACB**
227 We used a dual viral tracing strategy (diagram of approach in Fig. 5A; representative LS
228 injection site in Fig. 5B) to identify downstream targets of LS-projecting CA1v neurons. Results
229 revealed that the mPFC (Fig. 5C), the LHA (Fig. 5D) and the nucleus accumbens (ACB; Fig. 5E)
230 are among the strongest second-order targets of the CA1v to LS-projecting neurons. Quantitative
231 analyses using a custom built data-entry platform (Axiome C, created by JDH) are summarized
232 graphically for a representative animal on a brain flatmap summary diagram (Fig. 5F) for the
233 hemisphere ipsilateral (top) and contralateral (bottom) to the injection sites. The data are also
234 summarized in tabular form in Supplementary Table 1.
235
236 **DISCUSSION**
237 Memory for the physical location of a food source is adaptive for maintaining adequate
238 energy supply for reproduction and survival. However, the neural circuits mediating this
239 complex behavior are not well understood as research on visuospatial memory has
240 predominantly used tasks with either aversive or neutral/passive reinforcement. The present
241 study identified a specific monosynaptic CA1v to LS pathway as a necessary substrate for food-
242 motivated spatial memory using a newly developed foraging task. Moreover, the selectivity of
243 the CA1v-LS pathway in mediating spatial memory for food location is supported by results
244 showing that disconnection of this pathway did not affect performance in an escape-motivated
245 spatial memory task of comparable difficulty conducted in the same apparatus, anxiety-like
246 behavior, or olfactory and social-based appetitive memory. Viral pathway tracing identified that
247 LS-projecting CA1v neurons also send collateral projections to the mPFC, however, functional
248 disconnection of CA1v-mPFC signaling did not impair spatial memory for food location.

249 Utilization of an anterograde multisynaptic viral tracing approach and quantitative forebrain-
250 wide axon mapping analyses revealed that the CA1v-LS pathway sends second-order projections
251 to various feeding and reward-relevant neural substrates such as the LHA, ACB, and mPFC.
252 Collectively, these data establish monosynaptic CA1v to LS signaling as essential for spatial
253 memory-based foraging behavior, and we further identify a neural network of interconnected
254 feeding-relevant substrates that are collateral and/or downstream targets of this pathway.
255 Historically, the hippocampus has been divided into the dorsal and ventral subregions
256 that have both distinct and overlapping functions, anatomical connections, and genetic and
257 receptor expression profiles (12, 13, 17, 31, 43). The HPCd has been predominantly implicated
258 in facilitating spatial memory, whereas the HPCv is linked with stress responses, affective
259 behavior, and energy balance. However, the HPCv also plays a role in spatial memory,
260 particularly for goal-directed navigation. Consistent with present results, a recent study found
261 that both the HPCd and HPCv were critical for food reward-directed spatial navigation in an
262 obstacle-rich complex environment (44). Under some testing conditions, spatial learning and
263 memory in an aversive reinforcement-based water maze also requires both subregions of the
264 HPC (45). Similarly, whole-brain analysis of blood flow in rats during retrieval of spatial
265 memory in an aversive reinforcement-based Barnes maze task revealed increased activation in
266 the CA1d and CA1-3v in trained animals compared to controls (46). These results indicate that
267 spatial processing in the hippocampus is organized longitudinally, and that both HPCd and HPCv
268 are important for goal-directed spatial navigation. Here we extend these findings by revealing
269 that the HPCv, and more specifically, CA1v to LS signaling, is preferentially biased to
270 processing food-reinforcement based spatial memory.
271 Septohippocampal circuitry, which includes extensive connections between the
272 hippocampus (HPCd and HPCv) and septal nuclei (LS and medial), has been studied in the
273 context of a variety of behaviors, including, memory, stress and anxiety. HPCv-LS connections,
274 in particular, are linked with anxiety-like behavior. Transient pharmacological inactivation of
275 ipsilateral projections from the HPCv to LS suppresses anxiety-like behavior in an elevated plus
276 maze task (40), while bilateral DREADDs-mediated manipulation of bilateral HPCv to LS
277 projections during the same task reveal distinct anxiogenic and anxiolytic populations of neurons
278 (39). These findings suggest that hippocampal effects on anxiety may be mediated by
279 functionally distinct populations in the HPCv that project to the LS, and further, are potentially

280 dependent on laterality. However, these studies differ from the present study in that both CA1v
281 and CA3v subregions of the HPCv were targeted. Though we did not find changes in anxiety-
282 like behavior after reversible of chronic disconnection of CA1v to LS, the inclusion of CA3v in
283 the work described above prevents direct comparisons to our own results. Overall, these studies
284 combined with present results are consistent with a framework that overlapping and divergent
285 functions of the HPCv to LS signaling in both feeding and emotional regulation are important for
286 modulating complex motivated behavior in accordance with cognitive input (47).

287 Present results identify the CA1v-LS pathway in coordinating food-motivated behavior
288 with learned spatial information. While the use of aversive reinforcement-based spatial memory
289 tasks are predominant, the radial arm maze has been used to investigate food-motivated spatial
290 reference memory (analogous to the spatial memory probe in the present study) and spatial
291 working memory using multiple consistently food-baited arms (48). Inconsistent with the present
292 results, a previous study utilizing a four-baited/four-unbaited version of the eight-arm radial
293 maze task found that NMDA-mediated lesions of the HPCd, but not HPCv, impair spatial
294 reference and working memory (49). Another study using the same working memory task
295 reported that complete HPC lesions impaired both spatial and working memory, whereas lesions
296 to either the HPCd, HPCv, or intermediate HPC had no effect on memory performance (50).
297 Future studies will need to address whether discrepancies between the present results and these
298 studies are based on the differences between the behavioral tasks and/or differences in loss of
299 function methodologies. With regards to the latter, we note that our chemogenetic and lesion
300 approaches offered far greater specificity (LS-projecting CA1v neurons vs. whole HPCv)
301 compared with these studies.

302 Our multisynaptic neuroanatomical results offer a framework for future work to examine
303 the broader anatomical circuitry involved in foraging-related behaviors. Utilizing dual viral
304 approaches and systematic forebrain-wide quantitative mapping analyses, our findings confirm
305 that the CA1v-LS pathway projects downstream to other neural substrates involved in feeding
306 and motivated behavior, including the LHA, ACB, and mPFC. Given that the LS-LHA pathway
307 has been shown to affect food intake (51), and that metabolic activity in the LS and ACB is
308 associated food anticipatory activity in rabbit pups (52), it is possible that the LHA and/or the
309 ACB are functional downstream targets of CA1v-LS signaling for coordinating foraging
310 behavior. It is unlikely, however, that the mPFC is a functional target of CA1v-LS signaling for

311 appetitive spatial memory control. For example, our contralesional CA1v-mPFC disconnection
312 approach, which did not affect appetitive spatial memory, not only disconnects all ipsilateral
313 direct HPCv to mPFC communication, but also all ipsilateral multisynaptic HPCv to mPFC
314 connections (including via LS). Consistent with this hypothesis, anterograde labeling
315 downstream of CA1v to LS projections was not observed in the contralateral mPFC. It is
316 possible, however, that CA1v → LS → mPFC signaling is relevant to other motivated behaviors.
317 While we examined food-motivated and escape-motivated spatial memory, functional analyses
318 of this circuit may be extended to drug-motivated, social-motivated, or water-motivated spatial
319 memory tasks.
320 Collectively, we identify a CA1v to LS pathway involved in foraging-related, but not
321 escape-motivated, spatial memory. Furthermore, the selectivity of this pathway to appetitive
322 spatial memory is supported by data showing that neither chronic nor reversible disruption of
323 CA1v to LS signaling influenced various other behavioral outcomes. We also systematically
324 characterized collateral and second-order projections of this pathway, which demonstrate
325 overlapping pathways coordinated in the higher-order control of energy balance. These data shed
326 light on the neural systems underlying complex motivated behaviors that require functional
327 connections of cognitive and feeding-relevant substrates.
328
329 **METHODS**
330
331 **Animals**
332 Adult male Sprague–Dawley rats (Envigo; 250-275g on arrival) were individually housed
333 in hanging wire cages with *ad libitum* access (except where noted) to water and chow (LabDiet
334 5001, LabDiet, St. Louis, MO) on a 12h:12h reverse light/dark cycle. All procedures were
335 approved by the University of Southern California Institute of Animal Care and Use Committee.
336
337 **General intracranial injection procedures**
338 Rats were anesthetized via an intramuscular injection of an anesthesia cocktail (ketamine
339 90mg/kg body weight [BW], xylazine, 2.8mg/kg BW and acepromazine and 0.72mg/kg BW)
340 followed by a pre-operative, subcutaneous injection of analgesic (ketoprofen, 5mg/kg BW). Post-
341 operative analgesic (subcutaneous injection of ketoprofen, 5mg/kg BW) was administered once

342 per day for 3 days following surgery. The surgical site was shaved and prepped with iodine and
343 ethanol swabs, and animals were placed in a stereotaxic apparatus for stereotaxic injections.
344 NMDA or viruses were delivered using a microinfusion pump (Harvard Apparatus, Cambridge,
345 MA, USA) connected to a 33-gauge microsyringe injector attached to a PE20 catheter and
346 Hamilton syringe. Flow rate was calibrated and set to 83.3nl/sec. Injectors were left in place for
347 2min post-injection to allow for complete delivery of the infusate. Specific viruses/drugs,
348 coordinates, and injection volumes for procedures are detailed below. Following the completion
349 of all injections, incision sites were closed using either surgical staples, or in the case of
350 subsequent placement of an indwelling cannula, simple interrupted sutures. Upon recovery from
351 anesthesia and return to dorsal recumbency, animals were returned to the home cage. All
352 behavioral procedures occurred 21 days after injections to allow for complete transduction and
353 expression of the viruses, or complete lesioning drugs. General intracranial injection procedures
354 were followed for all injection procedures below.
355
356 **Chronic lesions of the HPCv**
357 Lesion animals received bilateral excitotoxic HPCv lesions via intracranial injections of
358 N-methyl-d-aspartate (NMDA; 200nL per hemisphere) at the following coordinates at three
359 different sites along the rostrocaudal extent of the HPCv (53): [1] -4.8mm AP, +/-5.0mm ML, -
360 7.5mm DV, [2] -5.5mm AP, +/-4.5mm ML, -7.0mm DV, and [3] -6.1mm AP, +/-4.8mm ML, -
361 7.0mm DV with control animals receiving vehicle saline in the same location. The reference
362 points for AP and ML coordinates were defined at bregma, and the reference point for the DV
363 coordinate was defined at the skull surface at the target site.
364 Bilateral HPCv lesion brains were histologically evaluated for the correct placement of
365 lesions in 1 out of 5 series of brain tissue sections. Neurons were visualized using
366 immunohistochemistry for the neuron specific antigen NeuN (see Immunohistochemistry), with
367 a complete lesion indicated by a lack of neuronal staining in the HPCv target region. Here, n=0
368 animals were removed. Representative images in Fig. 1A.
369
370 **Acute and chronic disconnection of the CA1v to LS neural pathway**
371 Cre-dependent dual viral strategies were used to generate the following groups: [1] acute
372 chemogenetic disconnection of the CA1v to LS neural pathway (DREADDs; diagram of

373 approach in Fig. 2A), [2] chronic disconnection of the CA1v to LS neural pathway (caspase
374 lesion-induced; diagram of approach in Fig. 2B), and [3] a common/shared control group for
375 these two disconnection strategies.
376 Regardless of group, all animals received a bilateral AAV retro-cre injection in the LS
377 (AAV2[retro]-hSYN1-EGFP-2A- iCre-WPRE; 200nL per side) at the following stereotaxic
378 coordinates (53): +0.84mm AP, +/-0.5mm ML, −4.8mm DV. The reference points for all LS
379 coordinates were defined at bregma.
380 According to experimental group, animals received a different virus delivered to the
381 CA1v subregion of the HPCv. All viruses were administered to the CA1v at the following
382 stereotaxic coordinates (53): −4.9mm AP, +/-4.8mm ML, −7.8mm DV. The reference points for
383 AP and ML coordinates were defined at bregma, and the reference point for the DV coordinate
384 was defined at the skull surface at the target site.
385 *[1] DREADDs group for reversible inactivation of CA1v to LS:* To allow reversible
386 chemogenetic inactivation of the CA1v to LS neural pathway, one group of animals received a
387 bilateral CA1v injection of a cre-dependent virus to drive expression of inhibitory designer
388 receptors activated by designer drugs (DREADDs), (AAV-Flex-hm4Di-tdTomato). This dual
389 viral strategy drives expression of inhibitory DREADDs exclusively in LS-projecting CA1v
390 neurons, which enables acute inactivation of these neurons by injection of the DREADDs ligand,
391 clozapine-N-oxide (CNO), at the time of behavioral testing.
392 *[2] Caspase group for chronic inactivation of CA1v to LS:* To allow chronic
393 disconnection of the CA1v to LS neural pathway, a second group of animals received a bilateral
394 CA1v cre-dependent caspase virus (AAV1-Flex-taCasp3-TEVp; 200nL per side) mixed with a
395 cre-dependent reporter virus (AAV-flex-tdTomato; 200nL per side) for histological verification.
396 This dual viral strategy drives expression of the apoptosis-mediator molecule caspase exclusively
397 in LS-projecting CA1v neurons, which induces apoptotic cell death in these neurons while
398 leaving other CA1v neurons intact.
399 *[3] Common control:* A common control group was generated for both of these
400 experimental groups, with this group receiving a cre-dependent control AAV in the CA1v
401 (AAV-flex-tdTomato).
402 Immediately following viral injections, all animals were surgically implanted with a
403 unilateral indwelling intracerebroventricular (ICV) cannula (26-gauge, Plastics One, Roanoke,

404 VA) targeting the lateral ventricle (VL). Cannulae were implanted and affixed to the skull with
405 jeweler's screws and dental cement at the following stereotaxic coordinates: −0.9mm AP,
406 +1.8mm ML, −2.6mm DV. The reference points for AP and ML coordinates were defined at
407 bregma, and the reference point for the DV coordinate was defined at the skull surface at the
408 target site. Placement for the VL cannula was verified by elevation of blood glucose resulting
409 from an injection of 210µg (2µL) of 5-thio-D-glucose (5TG) using an injector that extended
410 2mm beyond the end of the guide cannula (54). A post-injection elevation of at least 100% of
411 baseline glycemia was required for subject inclusion. Animals that did not pass the 5TG test
412 were retested with an injector that extended 2.5mm beyond the end of the guide cannula and,
413 upon passing the 5TG test, were subsequently injected using a 2.5mm injector instead of a 2mm
414 injector for the remainder of the study. Prior to behavioral testing where noted, all animals
415 received an ICV 18mmol infusion (2uL total volume) of the DREADDs ligand clozapine N-
416 oxide (CNO) (55), rendering only DREADDs animals chemogenetically inactivated. CNO
417 injections were hand delivered using a 33-gauge microsyringe injector attached to a PE20
418 catheter and Hamilton syringe through the indwelling guide cannulae. Injectors were left in place
419 for 30sec to allow for complete delivery of the CNO.
420 Cre-dependent DREADD expression targeting LS-projecting neurons in CA1v was
421 evaluated based on localization of the fluorescent reporter tdTomato. Immunohistochemistry for
422 red fluorescent protein (RFP) was conducted to amplify the tdTomato signal (see
423 Immunohistochemistry). After histological analysis, animals were removed based on misses (n=3
424 for cohort 1; n=0 for cohort 2). Representative images in Figs. 2C&D.
425 Neuronal apoptosis due to activation of cre-dependent caspase targeting LS-projecting
426 neurons in CA1v was evaluated based on reduction of the fluorescent reporter tdTomato due to
427 neuron cell death compared with histological controls. Caspase brains (which received a retro-
428 cre virus in the LS in conjunction with an injection of cre-dependent caspase virus mixed with a
429 cre-dependent virus that drives a tdTomato fluorescent reporter in the CA1v) were compared to
430 histological control brains (that received a retro-cre virus in the LS in conjunction with only a
431 cre-dependent that drives a tdTomato fluorescent reporter in the CA1v, which was equivalently
432 diluted to match the caspase injections). In both groups, immunohistochemistry for red
433 fluorescent protein (RFP) was conducted to amplify the tdTomato signal (see
434 Immunohistochemistry). Confirmation of successful caspase activation in the CA1v was

435 evaluated by reduced tdTomato fluorescence in comparison to histological control animals.
436 Animals were removed based on incomplete caspase lesioning (n=0 for cohort 1; n=0 for cohort
437 2). Representative images in Supplementary Figs 2E&F.
438
439
440 **Identification of collateral targets of CA1v to LS projecting neurons**
441 Collateral targets of the CA1v to LS neural pathway were identified using a dual viral
442 approach (diagram of approach in Fig. 4A) where a retrograde vector was injected into the LS
443 (AAV2retro-hSyn1-eGFP-2A-iCre-WPRE; 200nL per side; coordinates as above), and a Cre-
444 dependent anterograde vector (AAV1-CAG-Flex-tdTomato-WPRE-bGH; 200nL per side;
445 coordinates as above) was injected in the CA1v. This latter injection drives tdTomato transgene
446 expression in CA1v neurons that project to the LS, which allows for brain-wide analyses of
447 collateral targets. After 3 weeks of incubation time to allow for complete transduction and
448 expression of the viruses, brains were collected, immunohistochemically processed, and imaged
449 as described below.
450
451 **Contralesional disconnection of the CA1v to mPFC neural pathway or the CA1v to LHA**
452 **neural pathway**
453 To functionally disconnect the CA1v to mPFC pathway (diagram of approach in Fig. 4E),
454 or the CA1v to LHA pathway (diagram of approach in Fig. 4J) lesion animals received a
455 unilateral excitotoxic CA1v lesion via an intracranial injection of NMDA (200nL) at the
456 following coordinates (34): −4.9mm AP, + or - 4.8mm ML (left/right counterbalanced to be
457 contralateral to mPFC or LH lesion within-animal), −7.8mm DV, with control animals receiving
458 vehicle saline injections in the same location. The reference points for AP and ML coordinates
459 were defined at bregma, and the reference point for the DV coordinate was defined at the skull
460 surface at the target site.
461 In addition to the CA1v lesion, CA1v to mPFC disconnect animals also received a
462 unilateral excitotoxic mPFC lesion via two intracranial injections of NMDA (100nL per
463 injection) at the following coordinates (53): [1] +2.7mm AP, + or - 0.7mm ML (left/right
464 counterbalanced to be contralateral to CA1v lesion within-animal), −5.3mm DV and [2] +3.0mm
465 AP, + or - 0.7mm ML (left/right counterbalanced to be contralateral to CA1v lesion within-

466 animal), −4.7mm DV, with control animals receiving vehicle saline in the same location. The
467 reference points for all mPFC coordinates were defined at bregma.
468 In addition to the CA1v lesion, CA1v to LHA disconnect animals also received a
469 unilateral excitotoxic LHA lesion via an intracranial injection of NMDA (100nL per injection) at
470 the following coordinates (53): +2.9mm AP, + or – 1.1mm ML (counterbalanced to be
471 contralateral to CA1v lesion within-animal), −8.9mm DV, with control animals receiving vehicle
472 saline in the same location. The reference points for all LHA coordinates were defined at
473 bregma.
474 Contralateral brains were histologically evaluated for the correct placement of lesions by
475 visualizing neurons using immunohistochemistry for the neuron specific antigen NeuN (see
476 Immunohistochemistry). A complete lesion was indicated by a lack of neuronal labeling in the
477 CA1v, mPFC, or LHA target regions as necessary. Here, n=0 animals were removed.
478
479
480 **Identification of second order targets of CA1v to LS projecting neurons**
481 To identify second order targets of CA1v to LS-projecting neurons (diagram of approach
482 in Fig. 5A), animals received a bilateral injection of a transsynaptic Cre-inducing anterograde
483 vector into CA1v (AAV1-hSyn-Cre-WPRE-hGH; 200nL per side; coordinates as above) that
484 drives expression of Cre in both first-order (CA1v injection site) and 2nd-order (but not 3rd-
485 order) neurons via transsynaptic virion release (56, 57). This was combined with a bilateral
486 injection of a Cre-dependent anterograde vector in the LS (AAV1-CAG-Flex-tdTomato-WPRE-
487 bGH; 200nL per side, coordinates as above). This latter injection allows for anterograde tracing
488 from 1st-order LS targets receiving synaptic input from CA1v. After 3 weeks of incubation time
489 to allow for complete transduction and expression of the viruses, brains were collected,
490 immunohistochemically processed, and imaged as described below.
491 Data were entered using a custom built data-entry platform (Axiome C, created by JDH)
492 built around Microsoft Excel software and designed to facilitate entry of data points for all gray
493 matter regions across their atlas levels as described in a rat brain reference atlas (Brain Maps 4.0,
494 Swanson, 2018). The Axiome C approach was used previously to facilitate the analysis of brain
495 gene-expression data (Hahn et al., 2019). An ordinal scale, ranging from 0 (absent) to 7 (very
496 strong), was used to record the qualitative weight of anterograde labeling. An average value was

then obtained for each region across its atlas levels for which data were available. These data are summarized graphically for a representative animal on a brain flatmap summary diagram (adapted from (58).

Food intake and body weight

For the day prior to surgery (day 0) and for two weeks thereafter, 24h chow intake was measured daily just prior to dark cycle onset to determine effects of experimental procedures on food intake. Spillage was accounted for daily by collecting crumbs onto Techboard paper placed under the cages of each animal. Additionally, animals were weighed daily just prior to dark cycle onset to determine effects of experimental procedures on body weight.

Appetitive spatial memory foraging task

To test visuospatial learning and memory for food reinforcement, we developed a novel spatial foraging task modified from the traditional Barnes maze procedure. Throughout this paradigm, animals were maintained at 85% free-feeding body weight. The paradigm involves an elevated gray circular platform (diameter: 122cm, height: 140 cm) consisting of 18 uniform holes (9.5cm diameter) spaced every twenty degrees around the outside edge. Under one of the holes is a hidden tunnel (38.73cm L x 11.43cm W x 7.62cm D and a 5.08cm step). Surrounding the table are distinct spatial cues on the wall (e.g. holiday lights, colorful shapes, stuffed unicorn) that are readily visible to the animal. In contrast to the traditional Barnes Maze where an animal uses the spatial cues to escape mildly aversive stimuli in the environment (e.g. bright light and loud sound), this task utilizes food as motivation, such that each hidden tunnel contained five 45mg sucrose pellets (Bio-Serv, Flemington, NJ). Additionally, a quiet white noise (60dB) was used to drown out background noise and floor lamps were used for low-level ambient lighting. On the first day, each animal underwent a habituation session consisting of 1min inside a transport bin under the table, 2min underneath the start box in the center of the table, and 3min inside the hidden tunnel with 5 sucrose pellets. During training, each rat was assigned a specific escape hole according to the position of the spatial cues with the location counterbalanced across groups. Animals were trained over the course of two trials per day for four days (five days in contralesional experiments) to learn to use the spatial cues in order to locate the correct hole with the hidden tunnel with sucrose pellets. Learning during training was scored via animal head

528 location tracking by AnyMaze Behavior Tracking Software (Stoelting Co., Wood Dale, IL). The
529 incorrect hole investigations prior to finding the correct hole with sucrose pellets ("errors before
530 correct hole") as well as time to finding the correct hole ("latency to correct hole") were
531 calculated as an average of the two trials per day, and examined across days of training. After the
532 conclusion of training, rats had a two-day break where no procedures occurred, then were tested
533 in a single 2min memory probe in which the hidden tunnel and sucrose pellets were been
534 removed. All animals received an ICV 18mmol infusion of CNO (2uL total volume) 1h prior to
535 the memory probe, rendering only DREADDs animals chemogenetically inactivated by CNO. In
536 the memory probe, the ratio of the correct hole plus adjacent hole investigations over the total
537 number of hole investigations were calculated via animal head location tracking by AnyMaze
538 Behavior Tracking Software (Stoelting, Wood Dale, IL). The correct holes plus adjacent over
539 total were compared between groups for the first minute and entire two minutes of the probe for
540 all tests. A diagram of the apparatus used for the spatial foraging task is included in Fig. 1B.
541
542 **Aversive spatial memory escape task (Barnes maze)**
543 To test visuospatial learning and memory for escape reinforcement, we used a modified
544 traditional Barnes maze procedure, which is a visuospatial-based escape task. Procedures were
545 exactly the same as above (Appetitive spatial memory foraging task, using the same apparatus, in
546 the same room, and with the same visuospatial cues) aside from the omission of the sucrose
547 pellets in the hidden tunnel, the presence of mildly aversive bright (120W) overhead lighting
548 instead of dim ambient lighting, and a mildly aversive loud white noise (75dB) instead of a quiet
549 white noise (60dB). This allowed us to test spatial learning and memory motivated by escape
550 from aversive stimuli in a nearly-identical procedure to our spatial foraging test for learning and
551 memory motivated by palatable food consumption. A diagram of the apparatus used for the
552 spatial escape task is included in Fig. 1B.
553
554 **Social transmission of food preference (STFP)**
555 To examine food-related memory based on social- and olfactory-based cues, we utilized
556 the social transmission of food preference (STFP) task and adapted protocols from (30, 38, 59,
557 60). Briefly, untreated normal adult rats are designated as 'Demonstrators', while experimental
558 groups are designated as 'Observers'. Demonstrators and Observers are habituated to a powdered

559 rodent chow [LabDiet 5001 (ground pellets), LabDiet, St. Louis, MO] overnight. 24h later,
560 Observers are individually paired with demonstrators and habituated to social interaction, where
561 rat pairs are placed in a social interaction arena (23.5cm W × 44.45cm L × 27cm H clear plastic
562 bin with Sani-chip bedding) and allowed to interact for 30min. Both Observers and
563 Demonstrators are returned to their home cages and food is withheld for 23hr prior to the social
564 interaction. For the social interaction, Demonstrators are given the opportunity to consume one
565 of two flavors of powdered chow (flavored with 2% marjoram or 0.5% thyme; counterbalanced
566 according to group assignments) for 30min in a room separate from Observers. Our pilot studies
567 and previous published work (60, 61) show that rats equally prefer these flavors of chow. The
568 Demonstrator rat is then placed in the social interaction arena with the Observer rat, and the pairs
569 are allowed to socially interact for 30min. Observers are then returned to their home cage and
570 allowed to eat *ad libitum* for 1h and then food is removed. The following day, the 23h food-
571 deprived Observer animals are given a home cage food preference test for either the flavor of
572 chow paired with the Demonstrator animal, or a novel, unpaired flavor of chow that is a flavor
573 that was not given to the Demonstrator animal (2% marjoram vs. 0.5% thyme; counterbalanced
574 according to group assignments). All animals received an ICV 18mmol infusion of CNO (2uL
575 total volume) 1h prior to the social interaction session, rendering only DREADDs animals
576 chemogenetically inactivated by CNO. Food intake (1h) was recorded with spillage accounted
577 for by collecting crumbs onto Techboard paper that is placed under the cages of each animal.
578 The % preference for the paired flavor is calculated as: 100*Demonstrator-paired flavored chow
579 intake/Demonstrator + Novel flavored chow intake. In this procedure, normal untreated animals
580 learn to prefer the Demonstrator paired flavor based on social interaction and smelling the breath
581 of the Demonstrator rat (30, 38, 59-61). A diagram of the STFP procedure is included in Fig. 3E.
582
583 **Zero maze**
584 The zero maze behavioral paradigm was used to evaluate anxiety-like behavior. The zero
585 maze apparatus used was an elevated circular track, divided into four equal length sections. Two
586 zones were open with 3 cm high curbs ('open zones'), whereas the two other zones were closed
587 with 17.5 cm high walls ('closed zones'). All animals received an ICV 18mmol infusion of CNO
588 (2uL total volume) 1h prior to testing, rendering only DREADDs animals chemogenetically
589 inactivated by CNO. Behavioral testing was performed during the light cycle. Animals were

590 placed in the maze for a single, 5min trial in which the location of the center of the animal's
591 body was measured by AnyMaze Behavior Tracking Software (Stoelting, Wood Dale, IL). The
592 apparatus was cleaned with 10% ethanol in between animals. During the trial, the number of
593 open zone entries and total time spent in open sections (defined as body center in open sections)
594 were measured, which are each indicators of anxiety-like behavior in this procedure. A diagram
595 of the zero maze apparatus is included in Fig. 3G.
596
597 **Open field**
598 An open field test was used to evaluate general levels of locomotor activity. The
599 apparatus used for the open field test was an opaque gray plastic bin (60cm × 56cm), which was
600 positioned on a flat table in an isolated room with a camera directly above the center of the
601 apparatus. Desk lamps were positioned to provide indirect lighting to all corners of the maze
602 such that the lighting in the box uniformly measured 30 lux throughout. All animals received an
603 ICV 18mmol infusion of CNO (2uL total volume) 1h prior to testing rendering only DREADDs
604 animals chemogenetically inactivated by CNO. Behavioral testing began at dark onset. At the
605 start of the 10min test, each animal was placed in the open field apparatus in the same corner
606 facing the center of the maze. The location of the center of the animal's body was measured with
607 the AnyMaze Behavior Tracking Software (Stoelting, Wood Dale, IL). Total distance traveled
608 was measured by tracking movement from the center of the animal's body throughout the test.
609
610 **Immunohistochemistry**
611 Rats were anesthetized via an intramuscular injection of an anesthesia cocktail (ketamine
612 90mg/kg BW xylazine, 2.8mg/kg BW and acepromazine and 0.72mg/kg BW) then transcardially
613 perfused with 0.9% sterile saline (pH 7.4) followed by 4% paraformaldehyde (PFA) in 0.1M
614 borate buffer (pH 9.5; PFA). Brains were dissected from the skull and post-fixed in PFA with
615 15% sucrose for 24h, then flash frozen in isopentane cooled in dry ice. Brains were sectioned to
616 30µm thickness on a freezing microtome. Sections were collected in 5-series and stored in
617 antifreeze solution at −20°C until further processing. General fluorescence IHC labeling
618 procedures were performed as follows. The antibodies and dilutions that were used are as
619 follows: [1] For lesion histology using the neuron-specific protein NeuN, the rabbit anti-NeuN
620 primary antibody (1:1000, Abcam) was used followed by a donkey anti-rabbit conjugated to

621 AF488 (1:500, Jackson Immunoresearch). [2] To amplify the native tdTomato signal for
622 neuroanatomical tracing or DREADDs histology, the rabbit anti-RFP primary antibody (1:2000,
623 Rockland) was used followed by a donkey anti-rabbit conjugated to Cy3 (1:500, Jackson
624 Immunoresearch). [3] To amplify the native GFP signal for LS injection site histology, the
625 chicken anti-GFP primary antibody (1:500, Abcam) was used followed by a donkey anti-chicken
626 secondary antibody conjugated to AF488 (1:500, Jackson Immunoresearch). Antibodies were
627 prepared in 0.02M potassium phosphate buffered saline (KPBS) solution containing 0.2% bovine
628 serum albumin and 0.3% Triton X-100 at 4 °C overnight. After thorough washing with 0.02M
629 KPBS, sections were incubated in secondary antibody solution. All secondary antibodies were
630 obtained from Jackson Immunoresearch and used at 1:500 dilution at 4°C, with overnight
631 incubations (Jackson Immunoresearch; West Grove, PA, USA). Sections were mounted and
632 coverslipped using 50% glycerol in 0.02 M KPBS and the edges were sealed with clear nail
633 polish. Photomicrographs were acquired using a Nikon 80i (Nikon DSQI1,1280X1024
634 resolution, 1.45 megapixel) under epifluorescence or darkfield illumination.
635
636 **Axon mapping**
637 Data were entered using a custom built data-entry platform (Axiome C, created by JDH)
638 built around Microsoft Excel software and designed to facilitate entry of data points for all gray
639 matter regions across their atlas levels as described in a rat brain reference atlas (53). The
640 Axiome C approach was used previously to facilitate the analysis of brain gene-expression data
641 (62). An ordinal scale, ranging from 0 (absent) to 7 (very strong), was used to record the
642 qualitative weight of anterograde labeling. An average value was then obtained for each region
643 across its atlas levels for which data were available. The data were summarized graphically for a
644 representative experiment on a brain flatmap summary diagram (adapted from (58)). The data are
645 also summarized in tabular form in Supplementary Table 1.
646
647 **Statistics**
648 Data are expressed as mean +/- SEM. Differences were considered to be statistically
649 significant at $p<0.05$. All variables were analyzed using the advanced analytics software package
650 Statistica (StatSoft, Tulsa, OK, USA). For all measures of food intake, body weight, and
651 errors/latency during spatial foraging and spatial escape task training, differences between

652 groups were evaluated using two-way repeated measures ANOVAs (treatment x time). For
653 lesion experiments, measures during spatial foraging and spatial escape task probes, differences
654 between groups were evaluated using two-tailed independent two-sample Student's t-tests. For
655 CA1v to LS disconnection experiments, measures during spatial foraging and spatial escape task
656 probes, the STFP paradigm, the zero maze paradigm, and the open field test, differences between
657 groups were evaluated using one-way ANOVAs. Significant ANOVAs were analyzed with a
658 Fisher's LSD posthoc test where appropriate. Outliers were identified as being more extreme
659 than the median +/- 1.5 * interquartile range. For all experiments, assumptions of normality,
660 homogeneity of variance (HOV), and independence were met where required.
661
662 **CONFLICT OF INTEREST**
663 No conflicts of interest.
664
665 **ACKNOWLEDGEMENTS**
666 This work was supported by National Institute of Diabetes and Digestive and Kidney Diseases
667 grants: DK104897 to SEK, DK118944 to CML, and DK116558 to ANS. Clozapine-N-Oxide
668 was kindly provided by the National Institute of Mental Health. The authors are grateful to the
669 Kanoski lab undergraduates for their assistance in behavioral experiments and histology.
670
671

Figure 1

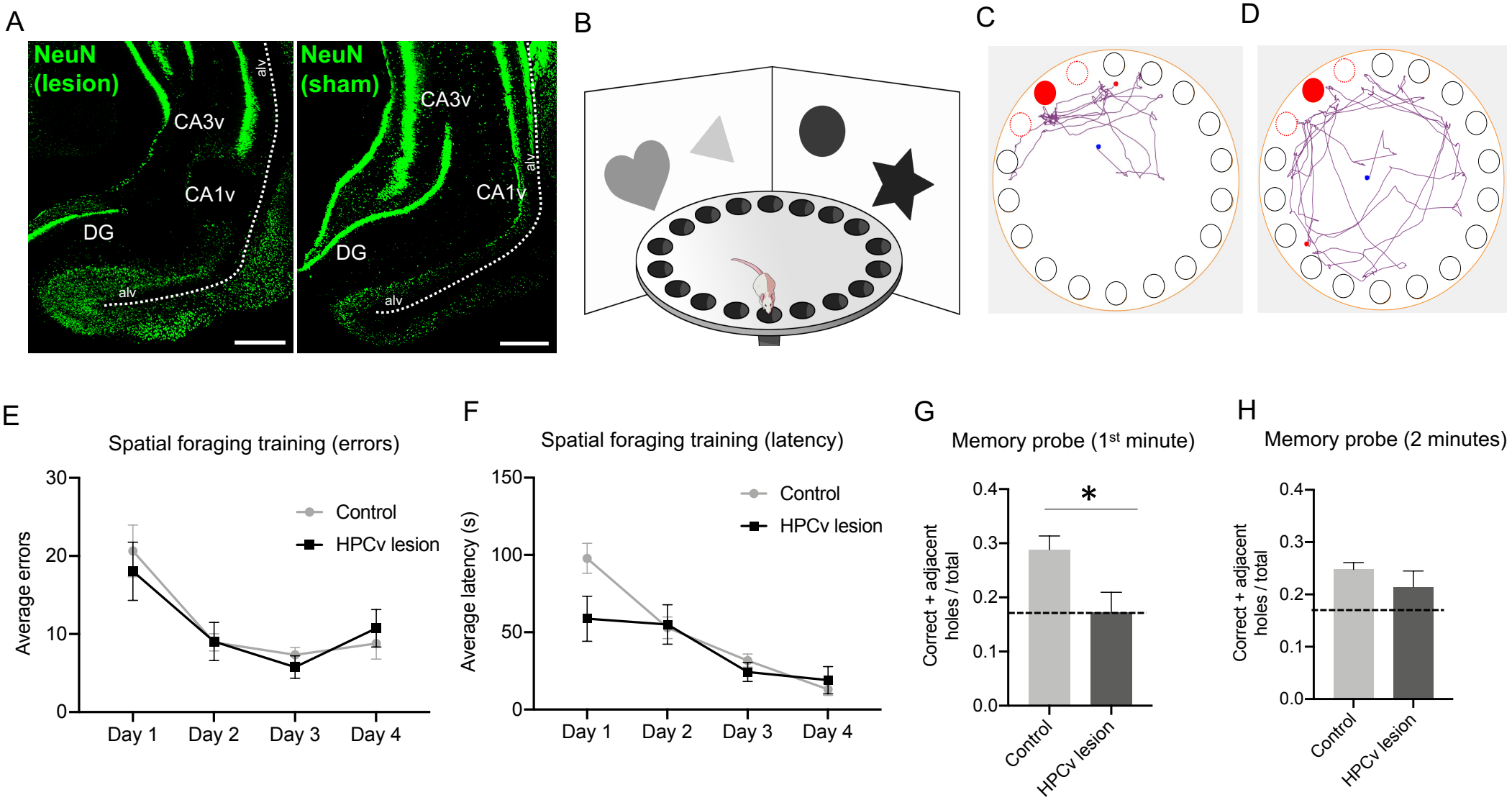
A
NeuN (lesion)
CA3v
CA1v
DG
alv
alv
NeuN (sham)
CA3v
CA1v
DG
alv
alv
B
C
D
E
Spatial foraging training (errors)
Average errors
30
20
10
0
Control
HPCv lesion
Day 1
Day 2
Day 3
Day 4
F
Spatial foraging training (latency)
Average latency (s)
150
100
50
0
Control
HPCv lesion
Day 1
Day 2
Day 3
Day 4
G
Memory probe (1st minute)
Correct + adjacent holes / total
0.4
0.3
0.2
0.1
0.0
*
Control
HPCv lesion
H
Memory probe (2 minutes)
Correct + adjacent holes / total
0.4
0.3
0.2
0.1
0.0
Control
HPCv lesion

672 **Figure 1. Bilateral HPCv lesions impair spatial memory for food location.** Representative
673 HPCv lesion histology with NeuN immunohistochemistry (A; scale bars 500μm). Spatial
674 foraging task apparatus (B). Representative navigation paths of a control animal preferentially
675 investigating correct (filled red) and adjacent holes (outlined orange) during spatial foraging
676 memory probe (C). Representative navigation path of HPCv lesioned animal during spatial
677 foraging memory probe (D). Bilateral HPCv lesions did not impair learning of the spatial
678 foraging task compared to controls, as measured by errors before locating correct hole during
679 task training (E) and latency to locate correct hole during task training (F). Bilateral HPCv
680 lesions impaired retention of the spatial foraging task, as measured by the ratio of investigation
681 of correct plus adjacent holes over total investigated during the first minute of the task ($p<0.05$;
682 G). There were no group differences observed when evaluated over the entire two minutes of the
683 task (H). Dotted line indicates chance performance level (0.167). For graphs 1D-G, lesion n = 11,
684 control n = 18. All values expressed as mean +/- SEM.
685
686

Figure 2

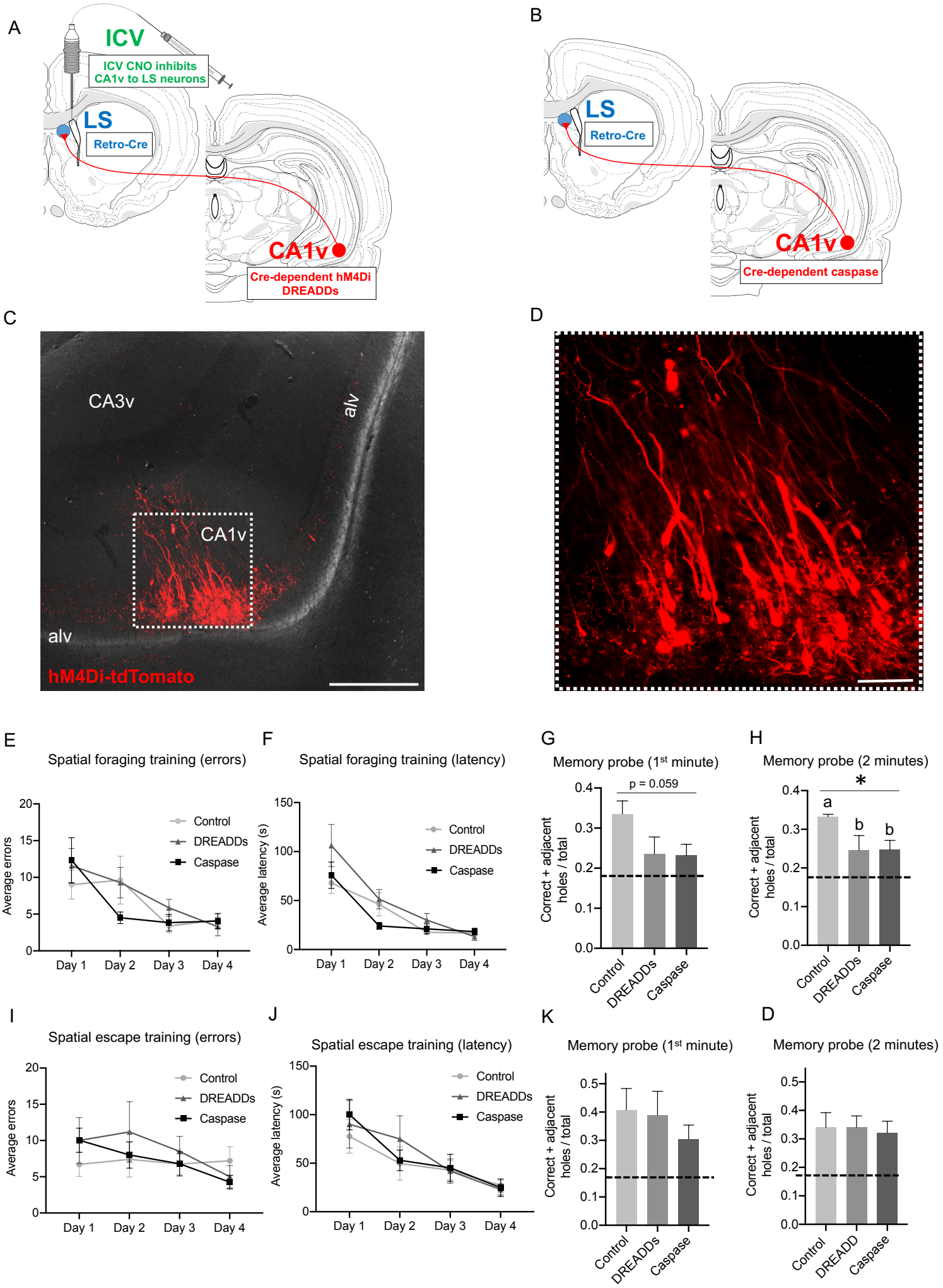
A
ICV
ICV CNO inhibits CA1v to LS neurons
LS
Retro-Cre
CA1v
Cre-dependent hM4Di DREADDs
B
LS
Retro-Cre
CA1v
Cre-dependent caspase
C
CA3v
alv
CA1v
alv
hM4Di-tdTomato
D
E
Spatial foraging training (errors)
Average errors
Control
DREADDs
Caspase
Day 1
Day 2
Day 3
Day 4
F
Spatial foraging training (latency)
Average latency (s)
G
Memory probe (1st minute)
p = 0.059
Correct + adjacent holes / total
H
Memory probe (2 minutes)
*
a
b
b
I
Spatial escape training (errors)
J
Spatial escape training (latency)
K
Memory probe (1st minute)
D
Memory probe (2 minutes)
DREADD

Figure 2. Reversible and chronic CA1v to LS neural disconnection impairs spatial memory for food location but not for escape location. Diagram of dual viral approach using a cre-dependent inhibitory DREADDs approach to reversibly disconnect CA1v to LS neural pathway (A). Diagram of dual viral approach using a cre-dependent caspase approach to chronically disconnect CA1v to LS neural pathway (B). Representative injection site in CA1v demonstrating LS-projecting neurons infected with inhibitory DREADDs, which simultaneously drives expression of a fluorescent tdTomato transgene (C, D; scale bars 500µm and 100µm, respectively). Neither reversible (DREADDs) nor chronic (caspase) disconnection of the CA1v to LS pathway impaired learning of the spatial foraging task compared to controls, as measured by errors before correct hole during task training (E) and latency to correct hole during task training (F). Both reversible and chronic disconnection of the CA1v to LS pathway impaired retention of the spatial memory foraging task as measured by the ratio of investigation of correct plus adjacent holes over total investigations during entire two minutes of the task ($p<0.05$; H). During the first minute of the task, there was a trend toward impaired learning in the disconnection groups, but this effect did not reach statistical significance ($p=0.059$; G). In contrast, disconnection of the CA1v to LS pathway either reversibly (DREADDs) or chronically (caspase) did not impair performance on the spatial escape task. There were no differences in learning as measured by errors before correct hole during task training (I) and latency to correct hole during task training (J). Unlike the spatial foraging task, retention of the spatial escape task was not impaired by reversible nor chronic disconnection of the CA1v to LS pathway (K, L). For graphs 2E-H (CA1v to LS disconnect cohort 1), DREADDs n=6, caspase n=10, control n=8. For graphs 2I-L (CA1v to LS disconnect cohort 2), DREADDs n=8, caspase n=12, control n=10. Dotted line indicates chance performance level (0.167). All values expressed as mean +/- SEM.

Figure 3

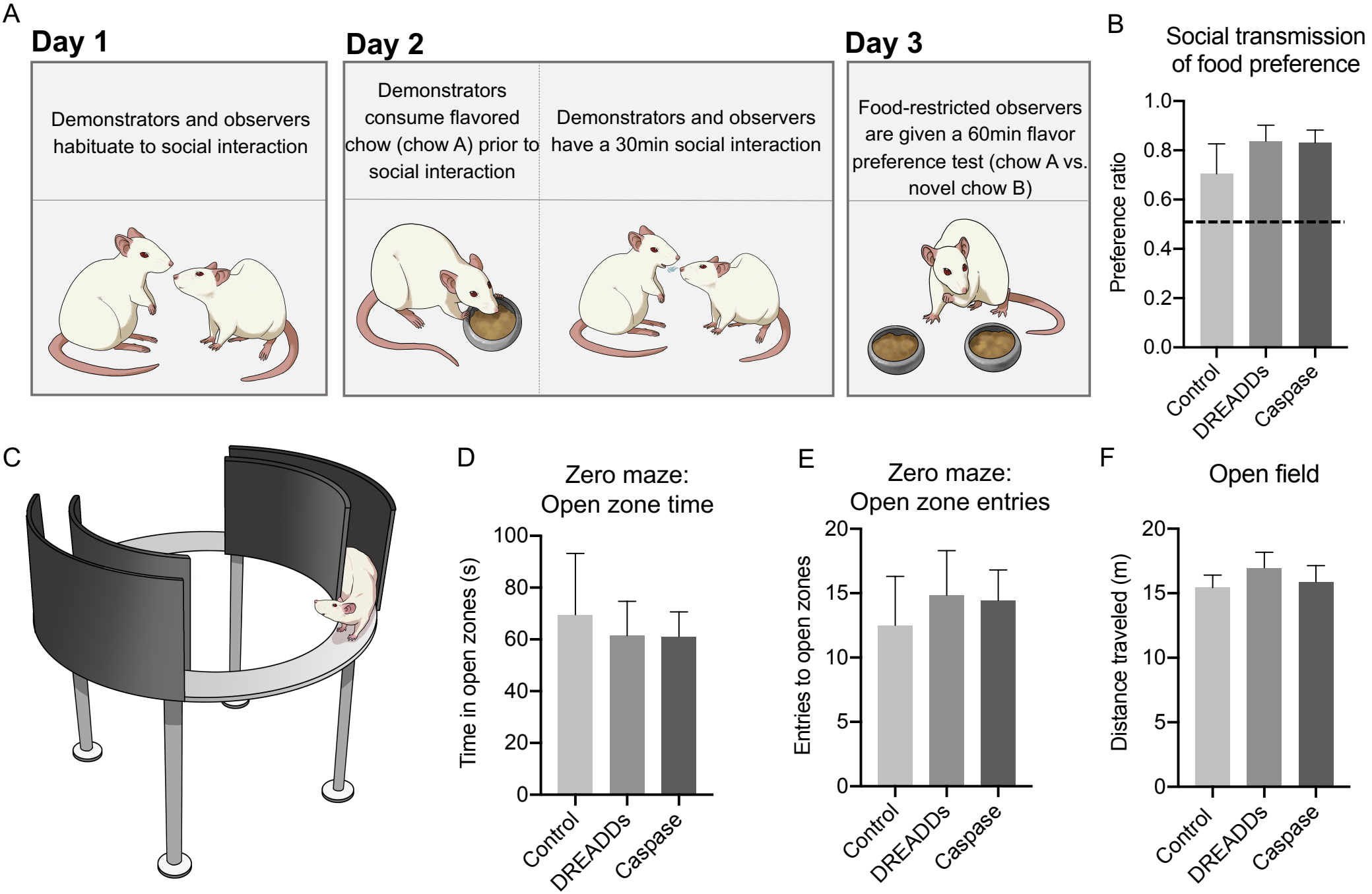
A
Day 1
Demonstrators and observers habituate to social interaction
Day 2
Demonstrators consume flavored chow (chow A) prior to social interaction
Demonstrators and observers have a 30min social interaction
Day 3
Food-restricted observers are given a 60min flavor preference test (chow A vs. novel chow B)
B
Social transmission of food preference
Preference ratio
1.0
0.8
0.6
0.4
0.2
0.0
Control
DREADDs
Caspase
C
D
Zero maze: Open zone time
Time in open zones (s)
100
80
60
40
20
0
Control
DREADDs
Caspase
E
Zero maze: Open zone entries
Entries to open zones
20
15
10
5
0
Control
DREADDs
Caspase
F
Open field
Distance traveled (m)
20
15
10
5
0
Control
DREADDs
Caspase

712 **Figure 3. Neither reversible nor chronic CA1v to LS neural disconnection impair spatial**
713 **memory for escape location, social transmission of food preference, anxiety-like behavior,**
714 **or general locomotor activity levels.** Diagram of the social transmission of food preference
715 (STFP) task (A). Neither reversible nor chronic disconnection of the CA1v to LS pathway impair
716 STFP learning compared to controls, as measured by a food preference ratio (B), with the dotted
717 line indicating chance preference level (0.50). Diagram of the zero maze apparatus (C). Anxiety-
718 like behavior was not influenced by reversible or chronic disconnection of the CA1v to LS
719 pathway compared to controls, as measured by performance in the zero maze task, specifically
720 time in open zones (D) and entries into open zones (E). Neither chronic nor reversible CA1v to
721 LS disconnection affected open field performance compared to controls, as measured by total
722 distance traveled (F). For graphs 3B, 3D, and 3E (CA1v to LS disconnect cohort 1), DREADDs
723 n=6, caspase n=10, control n=8. For graph 3F (CA1v to LS disconnect cohort 2), DREADDs
724 n=8, caspase n=12, control n=10. All values expressed as mean +/- SEM.
725
726

Figure 4

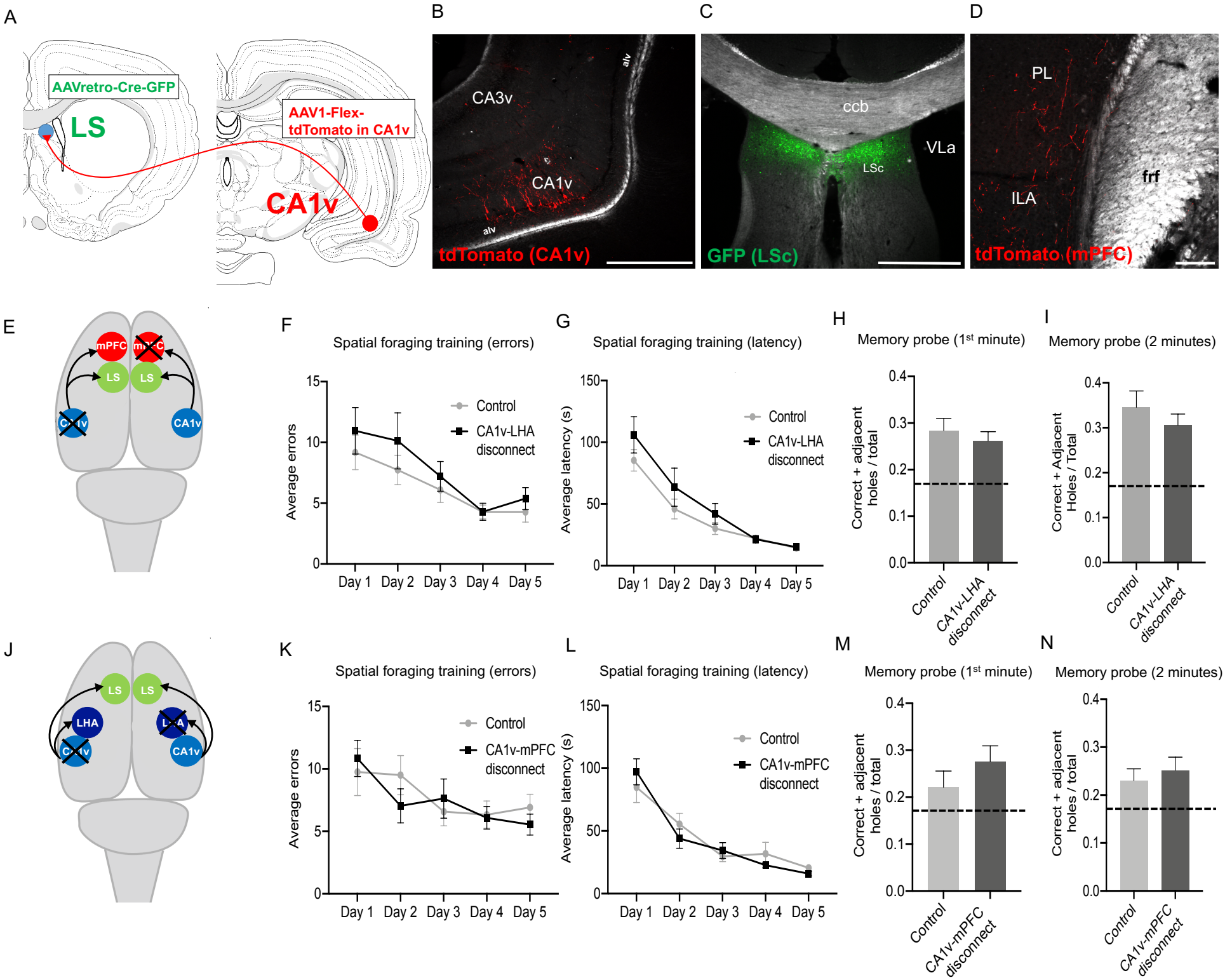
A
AAVretro-Cre-GFP
LS
AAV1-Flex-tdTomato in CA1v
CA1v
B
CA3v
alv
CA1v
alv
tdTomato (CA1v)
C
ccb
VLa
LSc
GFP (LSc)
D
PL
ILA
frf
tdTomato (mPFC)
E
mPFC
mPFC
LS
LS
CA1v
CA1v
F
Spatial foraging training (errors)
Average errors
Control
CA1v-LHA disconnect
Day 1 Day 2 Day 3 Day 4 Day 5
G
Spatial foraging training (latency)
Average latency (s)
Control
CA1v-LHA disconnect
Day 1 Day 2 Day 3 Day 4 Day 5
H
Memory probe (1st minute)
Correct + adjacent holes / total
Control
CA1v-LHA disconnect
I
Memory probe (2 minutes)
Correct + Adjacent Holes / Total
Control
CA1v-LHA disconnect
J
LS
LS
LHA
LHA
CA1v
CA1v
K
Spatial foraging training (errors)
Average errors
Control
CA1v-mPFC disconnect
Day 1 Day 2 Day 3 Day 4 Day 5
L
Spatial foraging training (latency)
Average latency (s)
Control
CA1v-mPFC disconnect
Day 1 Day 2 Day 3 Day 4 Day 5
M
Memory probe (1st minute)
Correct + adjacent holes / total
Control
CA1v-mPFC disconnect
N
Memory probe (2 minutes)
Correct + adjacent holes / total
Control
CA1v-mPFC disconnect

Figure 4. Neither CA1v to mPFC nor CA1v to LHA disconnection impairs spatial memory for food location. Diagram of dual viral approach to identify collateral targets of the CA1v to LS neural pathway (A). Representative CA1v injection site from collateral identification approach (B; scale bar 500µm). Representative LS injection site from collateral identification approach (C; scale bar 500µm). Representative image collateral axons of the CA1v to LS pathway located in the mPFC (D; scale bar 50µm). Diagram of contralesional approach to functionally disconnect the CA1v to mPFC neural pathway (E). Disconnection of the CA1v to mPFC neural pathway did not influence learning of the spatial foraging task compared to controls, as measured by errors before correct hole during training (F) and latency to correct hole during training (G). Disconnection of the CA1v to mPFC pathway did not influence retention of the spatial foraging task, as measured by during the first minute (H) and entire two minutes (I) of the memory probe. Diagram of contralesional approach to functionally disconnect the CA1v to LHA neural pathway (J). Disconnection of the CA1v to LHA neural pathway did not influence learning of the spatial foraging task compared to controls, as measured by errors before correct hole during training (K) and latency to correct hole during training (L). Disconnection of the CA1v to LHA pathway did not influence retention of the spatial foraging task, as measured by correct plus adjacent holes over total holes investigated during the first minute (M) and entire two minutes (N) of the memory probe. For graphs 4F-I, CA1v to mPFC disconnect n=12, control n=12. For graphs 4K-N, CA1v to LHA disconnect n=12, control n=11. All values expressed as mean +/- SEM.

Figure 5

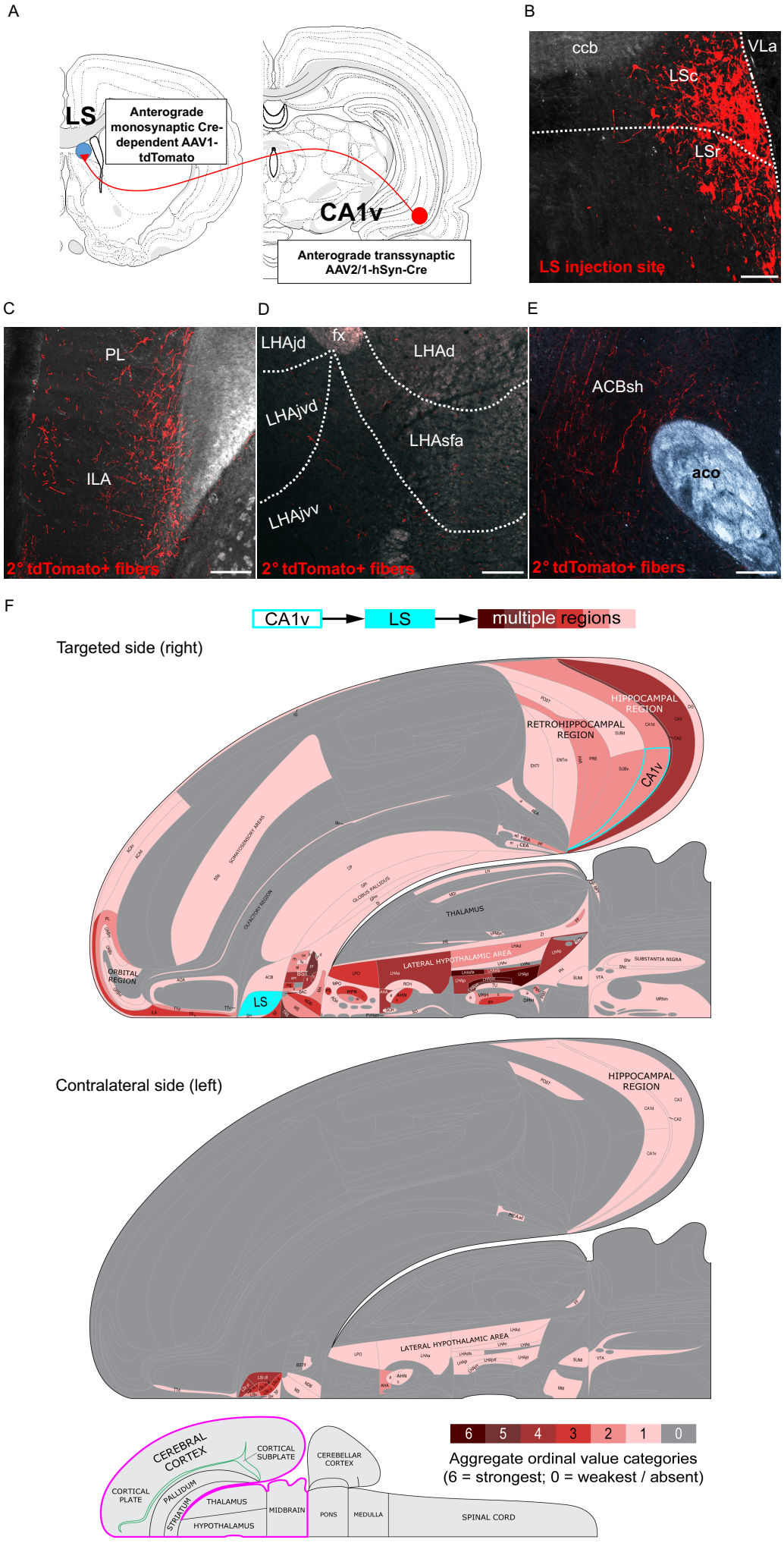
A
LS
Anterograde monosynaptic Cre-dependent AAV1-tdTomato
CA1v
Anterograde transsynaptic AAV2/1-hSyn-Cre
B
ccb
VLa
LSc
LSr
LS injection site
C
PL
ILA
2° tdTomato+ fibers
D
LHAjd
fx
LHAd
LHAjvd
LHAsfa
LHAjvv
2° tdTomato+ fibers
E
ACBsh
aco
2° tdTomato+ fibers
F
CA1v
LS
multiple regions
Targeted side (right)
HIPPOCAMPAL REGION
RETROHIPPOCAMPAL REGION
CA1v
THALAMUS
LATERAL HYPOTHALAMIC AREA
SUBSTANTIA NIGRA
ORBITAL REGION
LS
Contralateral side (left)
HIPPOCAMPAL REGION
LATERAL HYPOTHALAMIC AREA
CEREBRAL CORTEX
CORTICAL SUBPLATE
CEREBELLAR CORTEX
CORTICAL PLATE
PALLIDUM
STRIATUM
THALAMUS
HYPOTHALAMUS
MIDBRAIN
PONS
MEDULLA
SPINAL CORD
6 5 4 3 2 1 0
Aggregate ordinal value categories
(6 = strongest; 0 = weakest / absent)

749 **Figure 5. Identification of second-order neural projections downstream of CA1v to LS**
750 **projections.** Diagram of dual viral approach to identify brain regions that are second-order (2°)
751 targets of the CA1v to LS neural pathway (A). Representative LS injection site from second
752 order identification approach (B; scale bar 100µm). Representative image of second-order fibers
753 of the CA1v to LS pathway within the mPFC (C; scale bar 200µm). Representative image of
754 second-order fibers of the CA1v to LS pathway within the LHA (D; scale bar 200µm).
755 Representative image of second-order fibers of the CA1v to LS pathway within the ACB (E;
756 scale bar 200µm). Summary of the projection targets of LS neurons that receive input from
757 CA1v (F). The outputs of the right side of LS neurons receiving CA1v input are represented at
758 the macroscale (gray matter region resolution) on a partial flatmap representation of the rat
759 forebrain, adapted from (58). Connection weights are represented block colors for each region
760 following an ordinal scale ranging from weakest (0 = very weak or absent) to strongest (6 =
761 strong), as there were no 7 (very strong) values. The inset at lower left represents one side of the
762 brain with the part represented in the upper diagrams outlined in magenta.
763
764

765 **SUPPLEMENTARY INFORMATION**

766

767

Supplemental Figure 1

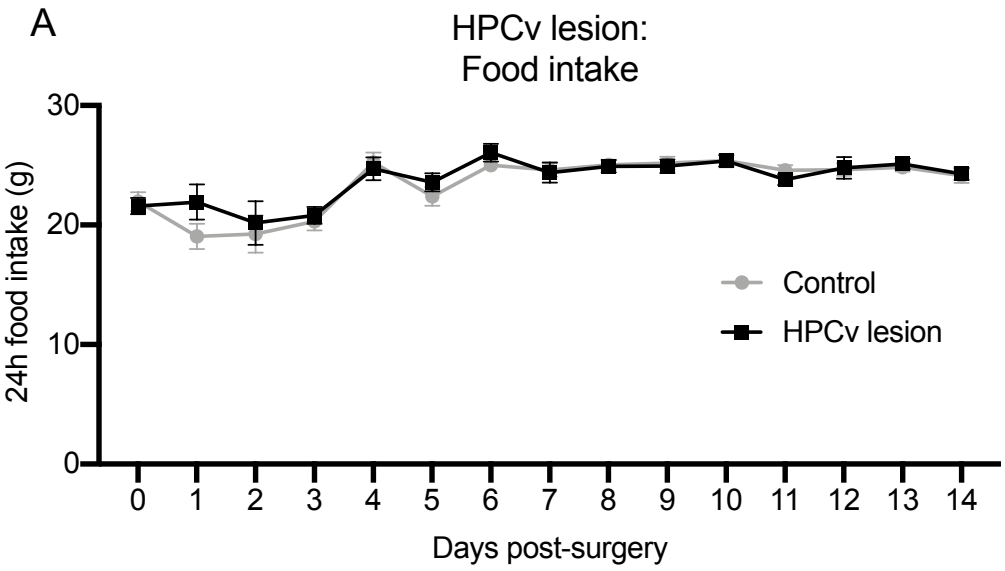

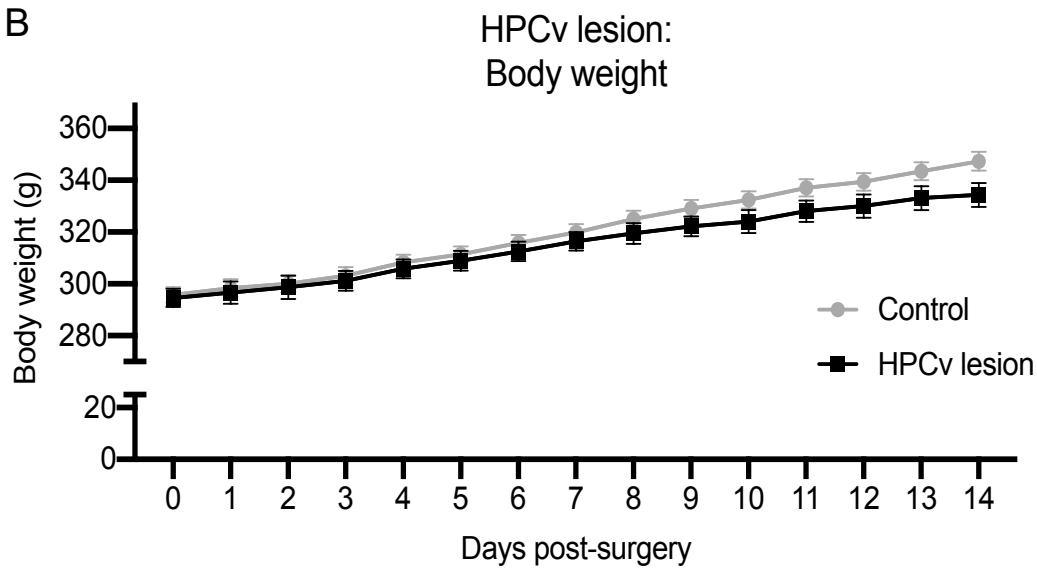

768 **Supplementary Figure 1. Effect of bilateral HPCv lesions on food intake and body weight.**
769 There were no effects on food intake (A) or body weight (B) of bilateral HPCv lesions compared
770 to controls. Lesion n = 11, control n = 18. All values expressed as mean +/- SEM.
771
772

Supplemental Figure 2

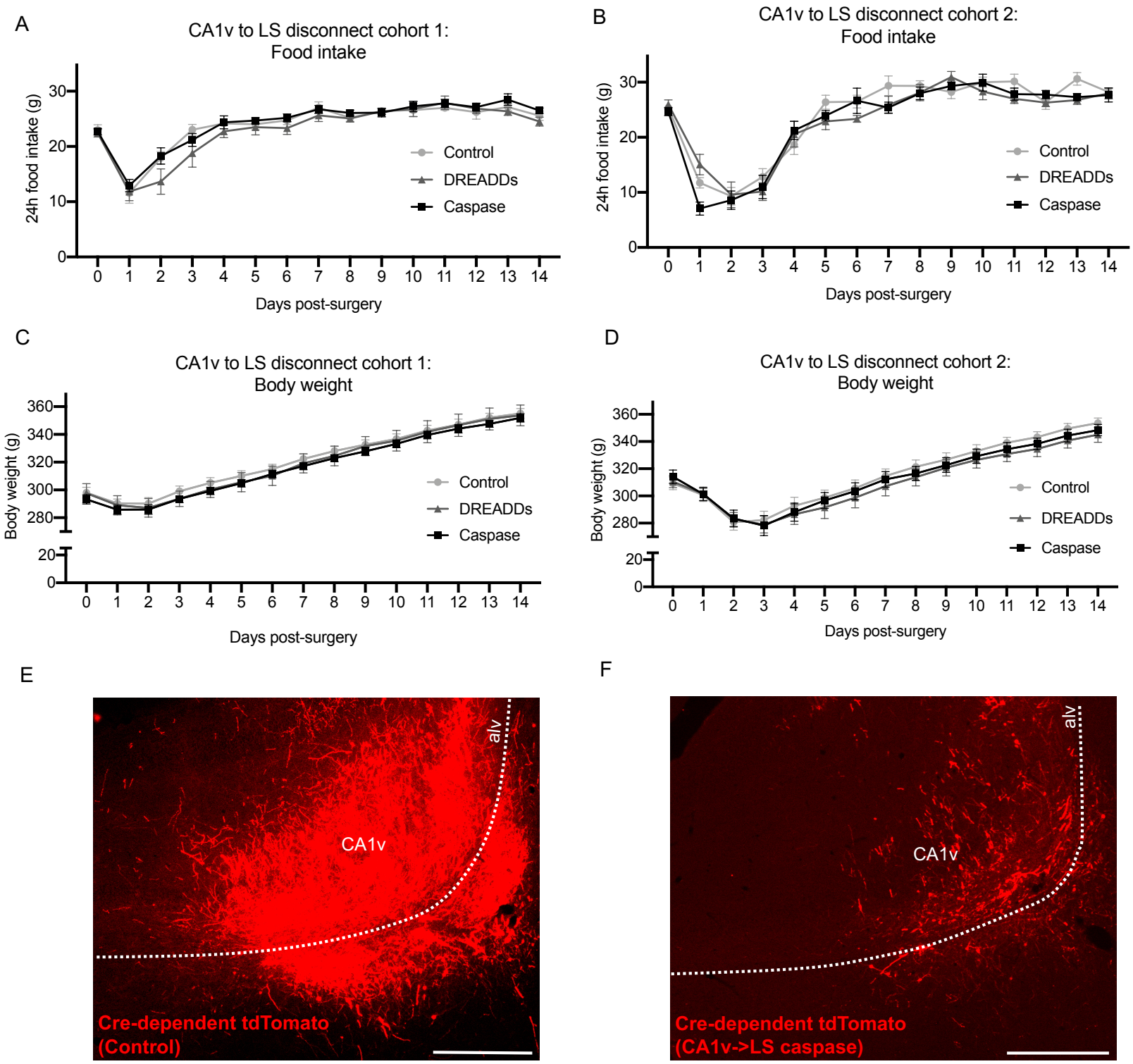

773 **Supplementary Figure 2. Effect of reversible and chronic disconnection of the CA1v to LS**
774 **neural pathway on food intake and body weight, and verification of the chronic approach.**
775 There were no effects on food intake (cohort 1: A; cohort 2: B) or body weight (cohort 1: C;
776 cohort 2: D) of reversible (DREADDs) or chronic (caspase) disconnection of the CA1v to LS
777 neural pathway compared to controls. Histological verification of the dual viral approach
778 demonstrates that cre-dependent tdTomato labeling of CA1v neurons induced by LS-origin retro-
779 cre is robust in a control animal (E), but reduced in an animal injected with cre-dependent
780 caspase combined with cre-dependent tdTomato due to caspase-induced cell death (F). For
781 graphs S1A-B (CA1v to LS disconnect cohort 1), DREADDs n=6, caspase n=10, control n=8.
782 For graphs S1C-D (CA1v to LS disconnect cohort 2), DREADDs n=8, caspase n=12, control
783 n=10. All values expressed as mean +/- SEM.
784
785

Supplemental Figure 3

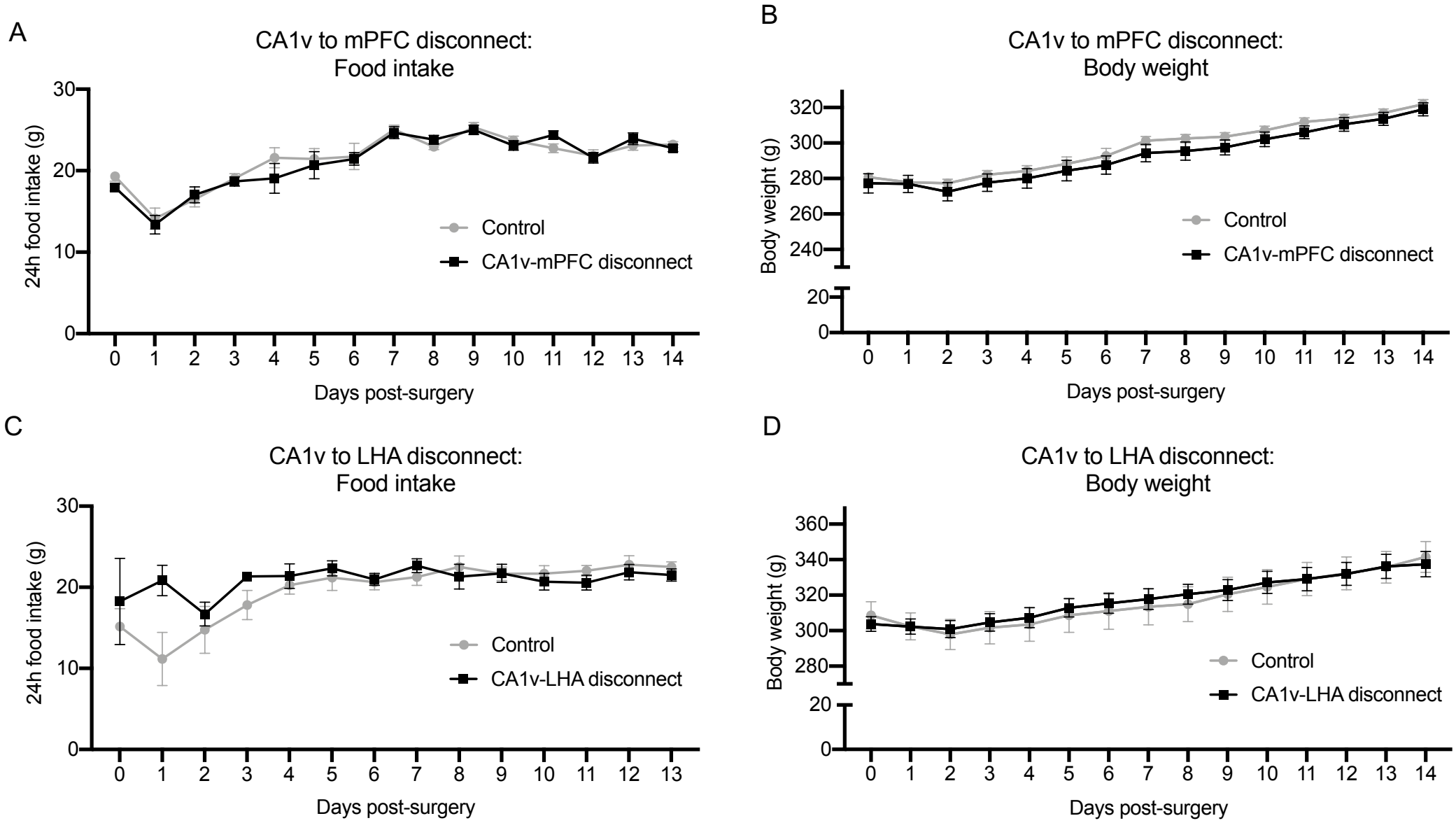

786 **Supplementary Figure 3. Effect of contralesional disconnection methods on food intake and**
787 **body weight.** There were no effects on food intake (A) or body weight (B) of contralesional
788 CA1v to mPFC compared to controls. CA1v to mPFC disconnect n=12, control n=12. There
789 were no effects on food intake (C) or body weight (D) of contralesional CA1v to LHA compared
790 to controls. CA1v to LHA disconnect n=12, control n=11. All values expressed as mean +/-
791 SEM.
792
793

Supplementary Table 1

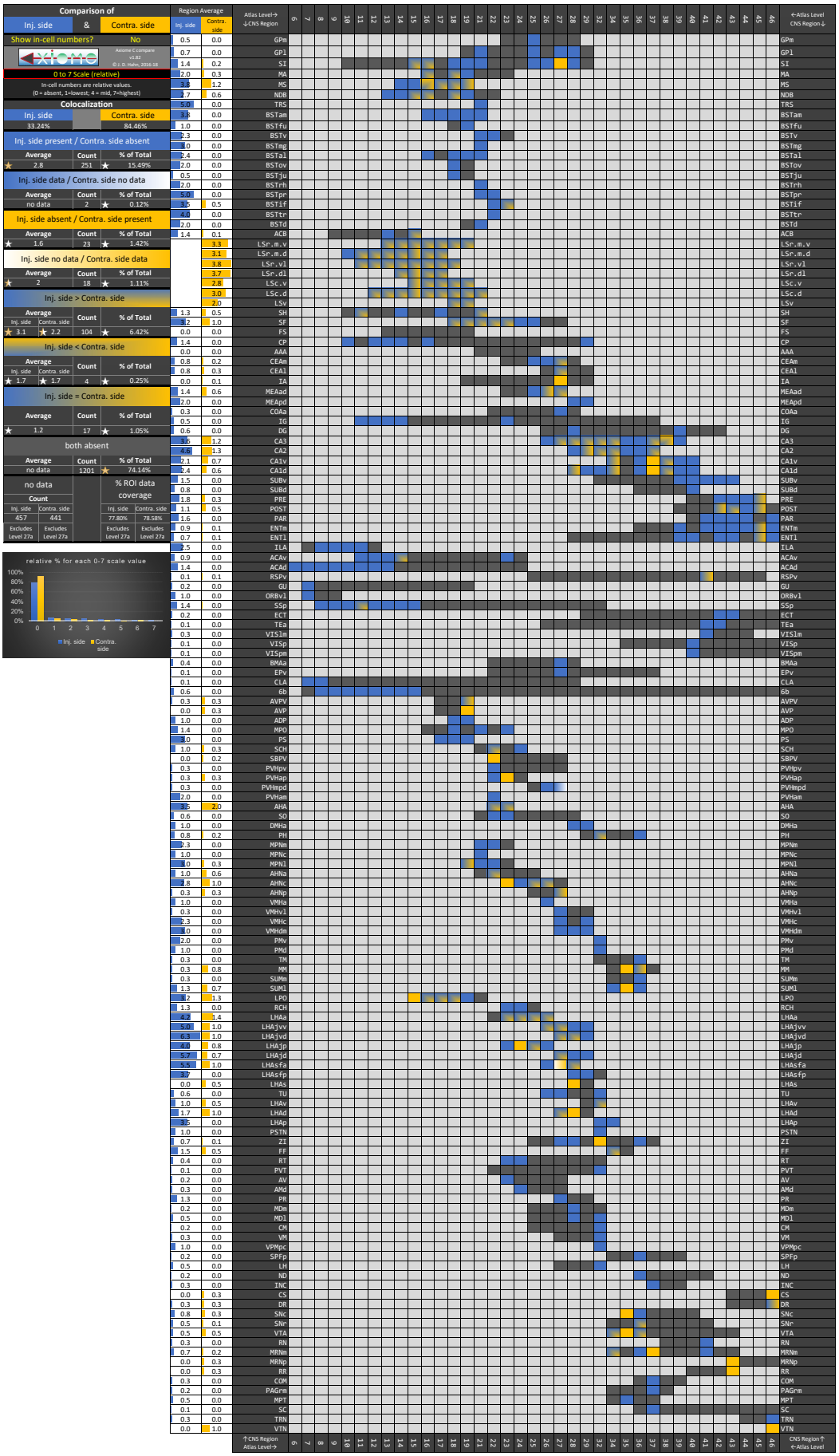

794 **Supplementary Table 1.** Summary table of the forebrain projection targets of LS neurons that
795 receive input from CA1v (derived the same raw data as the brain flatmap summary diagram in
796 Fig. 5F).
797
798

REFERENCES

1. R. G. M. Morris, U. Frey, "Hippocampal synaptic plasticity: Role in spatial learning or the automatic recording of attended experience?" in Burgess, Neil (Ed); Jeffery, Kathryn J (Ed); et al (1999) The hippocampal and parietal foundations of spatial cognition. (Oxford University Press, U Edinburgh, Ctr for Neuroscience, Edinburgh, Scotland London, 1999), pp. 220-246.
2. D. C. Rowland, Y. Roudi, M. B. Moser, E. I. Moser, Ten Years of Grid Cells. *Annu Rev Neurosci* **39**, 19-40 (2016).
3. R. Morris, Developments of a water-maze procedure for studying spatial learning in the rat. *Journal of neuroscience methods* **11**, 47-60 (1984).
4. C. A. Barnes, Memory deficits associated with senescence: a neurophysiological and behavioral study in the rat. *J Comp Physiol Psychol* **93**, 74-104 (1979).
5. J. O'Keefe, J. Dostrovsky, The hippocampus as a spatial map: preliminary evidence from unit activity in the freely-moving rat. *Brain research* (1971).
6. T. Hafting, M. Fyhn, S. Molden, M. B. Moser, E. I. Moser, Microstructure of a spatial map in the entorhinal cortex. *Nature* **436**, 801-806 (2005).
7. M. S. Fanselow, H.-W. Dong, Are the dorsal and ventral hippocampus functionally distinct structures? *Neuron* **65**, 7-19 (2010).
8. A. T. Keinath *et al.*, Precise spatial coding is preserved along the longitudinal hippocampal axis. *Hippocampus* **24**, 1533-1548 (2014).
9. K. B. Kjelstrup *et al.*, Finite scale of spatial representation in the hippocampus. *Science* **321**, 140-143 (2008).
10. L. de Hoz, J. Knox, R. G. Morris, Longitudinal axis of the hippocampus: both septal and temporal poles of the hippocampus support water maze spatial learning depending on the training protocol. *Hippocampus* **13**, 587-603 (2003).
11. J. Ferbinteanu, C. Ray, R. J. McDonald, Both dorsal and ventral hippocampus contribute to spatial learning in Long-Evans rats. *Neurosci Lett* **345**, 131-135 (2003).
12. M. B. Moser, E. I. Moser, Functional differentiation in the hippocampus. *Hippocampus* **8**, 608-619 (1998).
13. S. E. Kanoski, H. J. Grill, Hippocampus Contributions to Food Intake Control: Mnemonic, Neuroanatomical, and Endocrine Mechanisms. *Biol Psychiatry* **81**, 748-756 (2017).
14. P. G. Henke, Hippocampal pathway to the amygdala and stress ulcer development. *Brain Res Bull* **25**, 691-695 (1990).
15. K. G. Kjelstrup *et al.*, Reduced fear expression after lesions of the ventral hippocampus. *Proceedings of the National Academy of Sciences* **99**, 10825-10830 (2002).
16. S. Gaskin, A. Gamliel, M. Tardif, E. Cole, D. G. Mumby, Incidental (unreinforced) and reinforced spatial learning in rats with ventral and dorsal lesions of the hippocampus. *Behav Brain Res* **202**, 64-70 (2009).
17. M. S. Bienkowski *et al.*, Integration of gene expression and brain-wide connectivity reveals the multiscale organization of mouse hippocampal networks. *Nat Neurosci* **21**, 1628-1643 (2018).

841 18. R. Hannapel *et al.*, Postmeal Optogenetic Inhibition of Dorsal or Ventral Hippocampal
842 Pyramidal Neurons Increases Future Intake. *eNeuro* **6** (2019).
843 19. R. C. Hannapel, Y. H. Henderson, R. Nalloor, A. Vazdarjanova, M. B. Parent, Ventral
844 hippocampal neurons inhibit postprandial energy intake. *Hippocampus* **27**, 274-284
845 (2017).
846 20. B. K. Mani *et al.*, Neuroanatomical characterization of a growth hormone secretagogue
847 receptor-green fluorescent protein reporter mouse. *J Comp Neurol* **522**, 3644-3666
848 (2014).
849 21. J. M. Zigman, J. E. Jones, C. E. Lee, C. B. Saper, J. K. Elmquist, Expression of ghrelin
850 receptor mRNA in the rat and the mouse brain. *J Comp Neurol* **494**, 528-548 (2006).
851 22. I. Merchenthaler, M. Lane, P. Shughrue, Distribution of pre-pro-glucagon and glucagon-
852 like peptide-1 receptor messenger RNAs in the rat central nervous system. *J Comp*
853 *Neurol* **403**, 261-280 (1999).
854 23. S. E. Kanoski, S. M. Fortin, K. M. Ricks, H. J. Grill, Ghrelin signaling in the ventral
855 hippocampus stimulates learned and motivational aspects of feeding via PI3K-Akt
856 signaling. *Biol Psychiatry* **73**, 915-923 (2013).
857 24. S. E. Kanoski *et al.*, Hippocampal leptin signaling reduces food intake and modulates
858 food-related memory processing. *Neuropsychopharmacology* **36**, 1859-1870 (2011).
859 25. T. M. Hsu *et al.*, A hippocampus to prefrontal cortex neural pathway inhibits food
860 motivation through glucagon-like peptide-1 signaling. *Mol Psychiatry* **23**, 1555-1565
861 (2018).
862 26. T. M. Hsu, J. D. Hahn, V. R. Konanur, A. Lam, S. E. Kanoski, Hippocampal GLP-1 receptors
863 influence food intake, meal size, and effort-based responding for food through volume
864 transmission. *Neuropsychopharmacology* **40**, 327-337 (2015).
865 27. A. N. Suarez, C. M. Liu, A. M. Cortella, E. E. Noble, S. E. Kanoski, Ghrelin and Orexin
866 Interact to Increase Meal Size Through a Descending Hippocampus to Hindbrain
867 Signaling Pathway. *Biol Psychiatry* **87**, 1001-1011 (2020).
868 28. G. D. Petrovich, N. S. Canteras, L. W. Swanson, Combinatorial amygdalar inputs to
869 hippocampal domains and hypothalamic behavior systems. *Brain research reviews* **38**,
870 247-289 (2001).
871 29. C. De La Rosa-Prieto *et al.*, Subicular and CA1 hippocampal projections to the accessory
872 olfactory bulb. *Hippocampus* **19**, 124-129 (2009).
873 30. T. M. Hsu *et al.*, Hippocampus ghrelin receptor signaling promotes socially-mediated
874 learned food preference. *Neuropharmacology* **131**, 487-496 (2018).
875 31. L. W. Swanson, W. M. Cowan, An autoradiographic study of the organization of the
876 efferent connections of the hippocampal formation in the rat. *J Comp Neurol* **172**, 49-84
877 (1977).
878 32. P. Sweeney, Y. Yang, An excitatory ventral hippocampus to lateral septum circuit that
879 suppresses feeding. *Nat Commun* **6**, 10188 (2015).
880 33. A. Arszovszki, Z. Borhegyi, T. Klausberger, Three axonal projection routes of individual
881 pyramidal cells in the ventral CA1 hippocampus. *Front Neuroanat* **8**, 53 (2014).
882 34. P. Y. Risold, L. W. Swanson, Structural evidence for functional domains in the rat
883 hippocampus. *Science* **272**, 1484-1486 (1996).

35. R. Garcia, R. M. Vouimba, R. Jaffard, Spatial discrimination learning induces LTP-like changes in the lateral septum of mice. *Neuroreport: An International Journal for the Rapid Communication of Research in Neuroscience* **5**, 329-332 (1993).
36. R. Jaffard, R. M. Vouimba, A. Marighetto, R. Garcia, Long-term potentiation and long-term depression in the lateral septum in spatial working and reference memory. *J Physiol Paris* **90**, 339-341 (1996).
37. A. Carballo-Marquez, A. Vale-Martinez, G. Guillazo-Blanch, M. Marti-Nicolovius, Muscarinic receptor blockade in ventral hippocampus and prelimbic cortex impairs memory for socially transmitted food preference. *Hippocampus* **19**, 446-455 (2009).
38. R. A. Countryman, N. L. Kaban, P. J. Colombo, Hippocampal c-fos is necessary for long-term memory of a socially transmitted food preference. *Neurobiol Learn Mem* **84**, 175-183 (2005).
39. G. M. Parfitt *et al.*, Bidirectional Control of Anxiety-Related Behaviors in Mice: Role of Inputs Arising from the Ventral Hippocampus to the Lateral Septum and Medial Prefrontal Cortex. *Neuropsychopharmacology* **42**, 1715-1728 (2017).
40. N. L. Trent, J. L. Menard, The ventral hippocampus and the lateral septum work in tandem to regulate rats' open-arm exploration in the elevated plus-maze. *Physiology & behavior* **101**, 141-152 (2010).
41. J. C. Jimenez *et al.*, Anxiety Cells in a Hippocampal-Hypothalamic Circuit. *Neuron* **97**, 670-683.e676 (2018).
42. T. M. Hsu *et al.*, Hippocampus ghrelin signaling mediates appetite through lateral hypothalamic orexin pathways. *Elife* **4** (2015).
43. M. S. Fanselow, H. W. Dong, Are the dorsal and ventral hippocampus functionally distinct structures? *Neuron* **65**, 7-19 (2010).
44. M. Contreras, T. Pelc, M. Llofriu, A. Weitzenfeld, J. M. Fellous, The ventral hippocampus is involved in multi-goal obstacle-rich spatial navigation. *Hippocampus* **28**, 853-866 (2018).
45. S. L. T. Lee, D. Lew, V. Wickenheisser, E. J. Markus, Interdependence between dorsal and ventral hippocampus during spatial navigation. *Brain Behav* **9**, e01410 (2019).
46. D. P. Holschneider *et al.*, Cerebral perfusion mapping during retrieval of spatial memory in rats. *Behavioural brain research* **375**, 112116 (2019).
47. P. Sweeney, Y. Yang, Neural Circuit Mechanisms Underlying Emotional Regulation of Homeostatic Feeding. *Trends in endocrinology and metabolism: TEM* **28**, 437-448 (2017).
48. D. S. Olton, The radial arm maze as a tool in behavioral pharmacology. *Physiology & behavior* **40**, 793-797 (1987).
49. H. H. Pothuizen, W. N. Zhang, A. L. Jongen-Rêlo, J. Feldon, B. K. Yee, Dissociation of function between the dorsal and the ventral hippocampus in spatial learning abilities of the rat: a within-subject, within-task comparison of reference and working spatial memory. *The European journal of neuroscience* **19**, 705-712 (2004).
50. L. E. Jarrard, L. P. Luu, T. L. Davidson, A study of hippocampal structure-function relations along the septo-temporal axis. *Hippocampus* **22**, 680-692 (2012).

926 51. P. Sweeney, Y. Yang, An Inhibitory Septum to Lateral Hypothalamus Circuit That
927 Suppresses Feeding. *The Journal of neuroscience : the official journal of the Society for*
928 *Neuroscience* **36**, 11185-11195 (2016).
929 52. D. Olivo, M. Caba, F. Gonzalez-Lima, J. F. Rodríguez-Landa, A. A. Corona-Morales,
930 Metabolic activation of amygdala, lateral septum and accumbens circuits during food
931 anticipatory behavior. *Behav Brain Res* **316**, 261-270 (2017).
932 53. L. W. Swanson, Brain maps 4.0-Structure of the rat brain: An open access atlas with
933 global nervous system nomenclature ontology and flatmaps. *J Comp Neurol* **526**, 935-
934 943 (2018).
935 54. R. C. Ritter, P. G. Slusser, S. Stone, Glucoreceptors controlling feeding and blood glucose:
936 location in the hindbrain. *Science* **213**, 451-452 (1981).
937 55. E. E. Noble *et al.*, Hypothalamus-hippocampus circuitry regulates impulsivity via
938 melanin-concentrating hormone. *Nat Commun* **10**, 4923 (2019).
939 56. B. Zingg *et al.*, AAV-Mediated Anterograde Transsynaptic Tagging: Mapping
940 Corticocollicular Input-Defined Neural Pathways for Defense Behaviors. *Neuron* **93**, 33-
941 47 (2017).
942 57. A. N. Suarez *et al.*, Gut vagal sensory signaling regulates hippocampus function through
943 multi-order pathways. *Nat Commun* **9**, 2181 (2018).
944 58. J. D. Hahn, Swanson, L. W,. Bowman, I., Foster, N. N., Zingg, B., Bienkowski, M. S.,
945 Hintiryan, H., & Dong, H.-W. , An open access mouse brain flatmap and upgraded rat
946 and human brain flatmaps based on current reference atlases. *J. Comp. Neurol.* (2020).
947 59. R. A. Countryman, P. E. Gold, Rapid forgetting of social transmission of food preferences
948 in aged rats: relationship to hippocampal CREB activation. *Learn Mem* **14**, 350-358
949 (2007).
950 60. B. G. Galef, Jr., W. Y. Lee, E. E. Whiskin, Lack of interference in long-term memory for
951 socially learned food preferences in rats (Rattus norvegicus). *J Comp Psychol* **119**, 131-
952 135 (2005).
953 61. B. G. Galef, Jr., E. E. Whiskin, Socially transmitted food preferences can be used to study
954 long-term memory in rats. *Learn Behav* **31**, 160-164 (2003).
955 62. J. D. Hahn, O. Sporns, A. G. Watts, L. W. Swanson, Macroscale intrinsic network
956 architecture of the hypothalamus. *Proc Natl Acad Sci U S A* **116**, 8018-8027 (2019).
957